



HAL
open science

Condensation and evaporation processes during CB chondrite formation: Insights from Ge isotopes and highly siderophile element abundances

Guillaume Florin, Béatrice Luais, Olivier Alard, Tracy Rushmer

► **To cite this version:**

Guillaume Florin, Béatrice Luais, Olivier Alard, Tracy Rushmer. Condensation and evaporation processes during CB chondrite formation: Insights from Ge isotopes and highly siderophile element abundances. *Meteoritics and Planetary Science*, 2021, 56 (6), pp.1191-1211. 10.1111/maps.13698 . hal-03400295

HAL Id: hal-03400295

<https://hal.science/hal-03400295>

Submitted on 26 Nov 2021

HAL is a multi-disciplinary open access archive for the deposit and dissemination of scientific research documents, whether they are published or not. The documents may come from teaching and research institutions in France or abroad, or from public or private research centers.

L'archive ouverte pluridisciplinaire **HAL**, est destinée au dépôt et à la diffusion de documents scientifiques de niveau recherche, publiés ou non, émanant des établissements d'enseignement et de recherche français ou étrangers, des laboratoires publics ou privés.

Condensation and evaporation processes during CB chondrite formation: Insights from Ge isotopes and highly siderophile element abundances

Guillaume FLORIN ^{1,2*}, Béatrice LUAIS ¹, Olivier ALARD ^{2,3}, and Tracy RUSHMER ²

¹CNRS, CRPG, Université de Lorraine, Nancy F-5400, France

²Department of Earth and Planetary Sciences, Macquarie University, Sydney, New South Wales 2109, Australia

³Géosciences Montpellier, UMR 5243, CNRS & Université Montpellier, Montpellier 34095, France

*Corresponding author. E-mail: guillaume.florin@univ-lorraine.fr

(Received 16 September 2020; revision accepted 07 May 2021)

Abstract—We analyzed the highly siderophile element (HSE) contents and bulk Ge isotopic compositions of large metal grains in the CB chondrites Bencubbin (CB_a), Gujba (CB_a), and HaH 237 (CB_b). Our results suggest that the large grains were formed by the aggregation of smaller condensed grains, and the two Bencubbinite groups are distinguishable based on their bulk metal $\delta^{74/70}\text{Ge}$ mass-dependent isotopic values of $0.99 \pm 0.30\%$ (CB_a) and $-0.65 \pm 0.10\%$ (CB_b). Based on our observations of these three samples, the isotopic compositions of metal in CB_a chondrites are best explained by condensation at slow cooling rates in the center of an impact plume, whereas the metal in CB_b chondrites formed under fast cooling rates along the plume edges. We also analyzed the Ge contents and isotopic compositions of the core, intermediate, and rim fractions of two Gujba metal grains, which were separated by sequential digestion. These results show a gradual decrease in $\delta^{74/70}\text{Ge}$ and [Ge] from core to rim. We suggest that these $\delta^{74}\text{Ge}$ zonations result from near-equilibrium condensation and evaporation processes in a heterogeneous plume. We propose a model for their formation in which (1) small grains (to become grain cores) condensed at equilibrium; (2) these grains were transported to a warmer region of the plume where they reached temperatures lower than that of Fe-Ni condensation, but high enough for the rapid evaporation of Ge; (3) Ge evaporation followed by slow cooling enriched the grains in heavy Ge isotopes and the surrounding gas in light Ge isotopes; and (4) equilibrium recondensation of metal from the gas and around the small grains formed the light Ge isotopic zonations observed in grain rims.

INTRODUCTION

Among the carbonaceous chondrite groups, CB chondrites are unique as they (1) are enriched in Fe-Ni metal grains (60–80 vol% of the bulk chondrites), (2) lack any substantial matrix, (3) are enriched in refractory lithophile elements (i.e., with 50% condensation temperatures, T_{50} , above that of Mg, $T_{50}[\text{Mg}]$) by a factor of 1.3 and the refractory siderophile elements (i.e., with $T_{50} > T_{50}[\text{Pd}]$) by a factor of 13.7, and (4) are increasingly depleted in moderately volatile elements with increasing elemental volatility (Zipfel et al. 1998; Campbell et al. 2002). The metal (either kamacite or martensite) within bulk CB chondrites contains 4.1–14.8 wt% Ni (Weisberg et al.

2001) and has nearly solar Co/Ni ratios of ~ 0.045 (Anders and Grevesse 1989; Weisberg et al. 1990, 1995) and inversely correlated Cr-Ni contents (Weisberg et al. 2001). These features were first interpreted as the result of direct condensation from the solar nebular gas, thus reflecting the primitive nature of CB chondrites (Newsom and Drake 1979; Grossman et al. 1988; Meibom et al. 1999; Weisberg et al. 1999, 2001).

CB chondrites are divided into two subgroups: CB_a, mostly represented by Bencubbin, Gujba, and Weatherford; and CB_b, mostly represented by Hammadah al Hamra 237 (HaH 237), Queen Alexandra Range 94411 (QUE 94411), and Isheyevo (CH/CB_b, Ivanova et al. 2008). These two groups are distinguished based on the sizes, Ni contents, and elemental and

isotopic zonings of their metal grains (Weisberg et al. 2001). Compared with CB_a, CB_b chondrites contain generally smaller and zoned metal grains with rims enriched in Fe, Cr, and volatile elements (e.g., Au, Cu, Ge, Ga) and depleted in Ni, Co, and refractory elements (e.g., Re, Os, Ir) relative to their cores (Campbell et al. 2000, 2005; Weyrauch et al. 2019). The Fe, Ni, and Co distributions in CB_b metal are as expected from their fractional condensation from the solar nebular gas (Lodders et al. 2009). However, the distribution of platinum group elements (PGEs) relative to volatile elements (Campbell et al. 2001; Weyrauch et al. 2019) and Co and Ni concentrations in CB_b chondrites (Meibom et al. 1999; Petaev et al. 2001) are characteristic of condensation at high cooling rates in a dense, metal-rich environment (Campbell et al. 2002). Indeed, the low $\delta^{56}\text{Fe}$ and $\delta^{62}\text{Ni}$ values of the cores of CB_b metal grains relative to their rims (Zipfel and Weyer 2007; Richter et al. 2014; Weyrauch et al. 2019) reflect the kinetic condensation of the grains, during which light isotopes condensed first (Richter 2004).

Although the processes involved in CB chondrite formation remain debated, two main models have been suggested to interpret the observed chemical and isotopic patterns. Based on major element zonings, the first model suggests that CBs formed by equilibrium condensation from the solar nebular gas at total pressure $P^{\text{tot}} = 10^{-4}$ bar (Meibom et al. 1999; Petaev et al. 2001). However, several lines of evidence taken together contradict this model. (1) The partial pressure required for the condensation of siderophile elements is seven times that predicted for condensation from a gas of solar composition ($P^{\text{tot}} = 10^{-4}$ bar; Campbell et al. 2002). (2) The FeO-rich silicates in some CB chondrites are characteristic of more oxidizing conditions than those envisioned for the protoplanetary disk (Krot et al. 2000a, 2000b). This oxidizing behavior is also supported by the W and Mo depletions in zoned metal grains (Weyrauch et al. 2019). Additionally, FeO-rich silicates coexist with FeO-poor ones, implying various oxidation states. More importantly, (3) statistical astrophysical models based on the correlations between stellar mass and protoplanetary disk lifetime show that only 5% of the observed 0.4–1.4 M_{\odot} stars possess an accretion disk after 8 Myr, and that disk lifetime decreases by 2.6 times from 0.3 to 1 M_{\odot} (e.g., Yasui et al. [2014] and references therein). These models agree with the disappearance of the disk in our solar system by ≈ 4 –5 Myr after the formation of Ca–Al-rich inclusions (Connelly et al. 2012). Combined with the young and homogeneous ages of CB chondrites (4562.49 ± 0.21 Ma, Pb–Pb absolute ages, Krot et al. 2005; Bollard et al. 2015) that are indistinguishable from the ^{53}Mn – ^{53}Cr ages of chondrites and metal

(4562.5 ± 1.2 Ma; Yamashita et al. 2010), ^{129}I – ^{129}Xe ages of Gujba chondrules (4563.2 ± 1.3 Ma; Gilmour et al. 2009; Zhu et al. 2019), and ^{182}Hf – ^{182}W ages of Gujba metal (4562.2 ± 2.4 Ma; Kleine et al. 2005), CB chondrites seem to be the result of a single event that occurred shortly after the disappearance of the protoplanetary disk.

The second model argues for CB condensation from a vapor plume formed by the collision of two metal-rich planetary embryos (Kallemeyn et al. 2001; Krot et al. 2005), possibly of CH composition (Campbell et al. 2002). In this framework, the Fe and Ni isotopic compositions of metal grains suggest that unzoned metal grains (mostly CB_a) condensed at equilibrium in the center of the plume at low cooling rates and high partial gas pressure, whereas zoned grains (mostly CB_b) condensed in disequilibrium in the outer part of the plume at high cooling rates and low partial pressure (Weyrauch et al. 2019). However, this model is only partly supported by numerical modeling of an impact plume at $P^{\text{tot}} = 10^{-3}$ bar: good matches are observed for the Ir, Ni, Co, and Cr concentrations and Fe and Ni isotopic compositions of unzoned and zoned metal grains, yet these calculations also produce large Fe and Ni isotopic zonings in cogenetic silicates, which are not observed in CB chondrites (Fedkin et al. 2015). Moreover, the plume model cannot fully explain the compositions of CB chondrites without assuming an unreasonably large number of starting compositions (Fedkin et al. 2015). Thus, although the impact plume hypothesis appears plausible, some large discrepancies must be addressed.

Although some data are available on moderately volatile elements in the metal phase (e.g., Cr, Au, P, As, Cu, Ga, Sb, Ge, Sn, S; Kallemeyn et al. 1978; Campbell et al. 2002; Meibom et al. 2005; Weyrauch et al. 2019), the condensation model of CB chondrite formation is mostly based on major (Fe, Ni, Co) and refractory siderophile element (e.g., Re, Os, Ir) concentrations and isotopic compositions in metal grains. Consequently, this model only accounts for processes occurring at temperatures above that of Fe–Ni condensation (for solar composition, $T_{50} [\text{Fe–Ni}] \approx 1300$ K at $p_{\text{H}_2\text{O}}/p_{\text{H}_2} = 4.2 \times 10^{-4}$ atm; Lodders et al. 2009; Wood et al. 2019), and the dynamics of CB metal grain condensation at intermediate temperatures are less known. Nonetheless, processes occurring at intermediate temperatures are well evidenced by the occurrence of fine exsolutions of kamacite and taenite, named plessite, in the cores of some metal grains. These exsolution textures may result from prolonged reheating events ($T > 400$ °C) prior to accretion (Zhang et al. 1993; Meibom et al. 2005). In that case, because of their high condensation temperatures (e.g., $T_{50}[\text{Fe}] = 1334$ K), Fe

and Ni are not useful isotopic tracers of lower temperature processes. Therefore, it is necessary to study moderately volatile and siderophile elements that record intermediate- and low-temperature processes (i.e., $T_{50}[\text{S}] \leq T \leq T_{50}[\text{Fe}]$; Lodders et al. 2009) to fully understand volatile depletion and other low-temperature processes of metal formation and evolution prior to CB accretion.

Germanium is a moderately siderophile and volatile element that condenses in Fe-Ni alloy (Sears 1978; Wai and Wasson 1979) at $T_{50} = 883 \text{ K}$ and $p_{\text{H}_2\text{O}}/p_{\text{H}_2} = 4.2 \times 10^{-4} \text{ atm}$ (Lodders et al. 2009), and is therefore ideal for unraveling the low-temperature formation and evolution of CB chondrites. Germanium contents and isotopic compositions vary widely among meteorite groups and have been used to characterize iron meteorites (Wasson 1974; Luais 2007, 2012); impact volatilization (Luais 2007); and, more recently, ordinary chondrite formation (Florin et al. 2020). Therefore, we report a comprehensive Ge elemental and isotopic survey of the bulk metal and individual metal grains from CB_a and CB_b chondrites. We first measured the Ge isotopic compositions of the bulk metal in the selected CB_a and CB_b chondrites. Because our sample of Gujba (CB_a) contained full spherical metal grains, we sequentially digested them to measure rim-core variations in Ge content and isotopic composition. In addition, we performed in situ analyses of moderately siderophile element (MSE: W, Mo, As, Cu, Ag, Ga, Ge, Pb) and highly siderophile element (HSE: Re, Os, Ir, Ru, Rh, Pd, Pt, Au) concentrations in CB_a and CB_b metal grains to distinguish high-temperature processes from intermediate- and low-temperature processes. We use our elemental and isotopic results to discuss metal grain condensation processes and constrain and model the environments of CB_a and CB_b metal formation.

SAMPLE SELECTION AND PETROLOGIC DESCRIPTION

We selected two CB_a chondrites, Bencubbin and Gujba, and one CB_b , HaH 237, for this study. CB chondrites are very rare meteorites, and most have masses lower than 800 g. Because Ge contents are low in CB chondrites (usually $<1 \text{ ppm}$; Weyrauch et al. 2019), 300 mg of pure metal is required for Ge isotopic analyses. We were only able to obtain samples of Gujba (fragment of 1.2 g) and Bencubbin (fragment of 1.9 g) of sufficient mass from museums. To complete our data set, we purchased a $2 \times 1 \times 0.2 \text{ cm}$ slice (2.143 g) of HaH 237 from the owner of the main meteorite mass.

Whereas previous studies (e.g., Weyrauch et al. 2019) focused on small metal grains (180–600 μm), we studied larger ones ($>900 \mu\text{m}$). We present here a short

petrographic description of the studied CB metal grains; more details are available in previous studies (Grossman and Zipfel 2001; Weisberg et al. 2001; Rubin et al. 2003; Meibom et al. 2005). All samples were embedded in resin and polished with ethanol to avoid oxidation. The following mineralogical and petrographic observations were performed using an optical microscope.

In Bencubbin (CB_a), most metal grains range from 1 to 4 mm in diameter (Weisberg et al. 2001) and are elongated, probably due to impact compaction, as highlighted by the footprint of grains M1 in grain M2, and the basal flatter of grain M3 (Fig. 1A). Cr-rich troilite (up to 2 wt% Cr; Weisberg et al. 2001) occurs either as rounded or elongated inclusions in the largest metal grains (Fig. 1B) or as thin films outlining small relic metal grains within large ones (Fig. 1C) (Weisberg et al. 2001). Metal grains are surrounded by silicates and mantled by immiscible metal-silicate “interstitial impact melts” (Figs. 1B and 1D). These interstitial melts comprise sulfides (Cr-rich troilite) and Fe-Ni alloys and are interpreted as resulting either from the partial melting of the adjacent metal grains during impact (Weisberg et al. 2001), matrix melting (Meibom et al. 2005), or as a spontaneous fusion texture (Newsom and Drake 1979).

Our sample of Gujba (CB_a) shows the same texture as Bencubbin, except that its metal grains (also 1–4 mm in diameter) are nearly perfect spheres that show only slight evidence of preferential elongation in some samples (Rubin et al. 2003; Weisberg and Kimura 2010). The presence of high-pressure majorite-wadsleyite assemblages in this meteorite suggests that it experienced a pressure and temperature of $\approx 19 \text{ GPa}$ and $2000 \text{ }^\circ\text{C}$ in an impact shock (Weisberg and Kimura 2010). However, the lack of strong preferential elongation in our sample is not consistent with such impact, suggesting that the associated deformation was highly localized. Additionally, our Gujba sample shows more occurrences of small relic metal grains delimited by sulfide films within larger grains than does Bencubbin (Fig. 1I). Similar metal-sulfide textures have been previously described in Gujba metal grains (Weyrauch et al. 2019).

HaH 237 (CB_b) shows a complex assemblage of metal grains, metallic melts, and silicates (Fig. 1E). Except for three grains larger than 1 mm in size, most metal grains are smaller ($\sim 100\text{--}300 \mu\text{m}$) than those in CB_a samples (Fig. 1F) (Weisberg et al. 2001; Krot et al. 2002). Large metal grains are aggregates of smaller ones (Fig. 1G) (Weisberg et al. 2001), sometimes separated by Fe-Ni oxides; these large grains are less aggregated than those in CB_a samples (Fig. 1G). Rounded troilite inclusions occur in some of these small, aggregated metal grains (Figs. 1F and 1G). Silicate phases are (1)

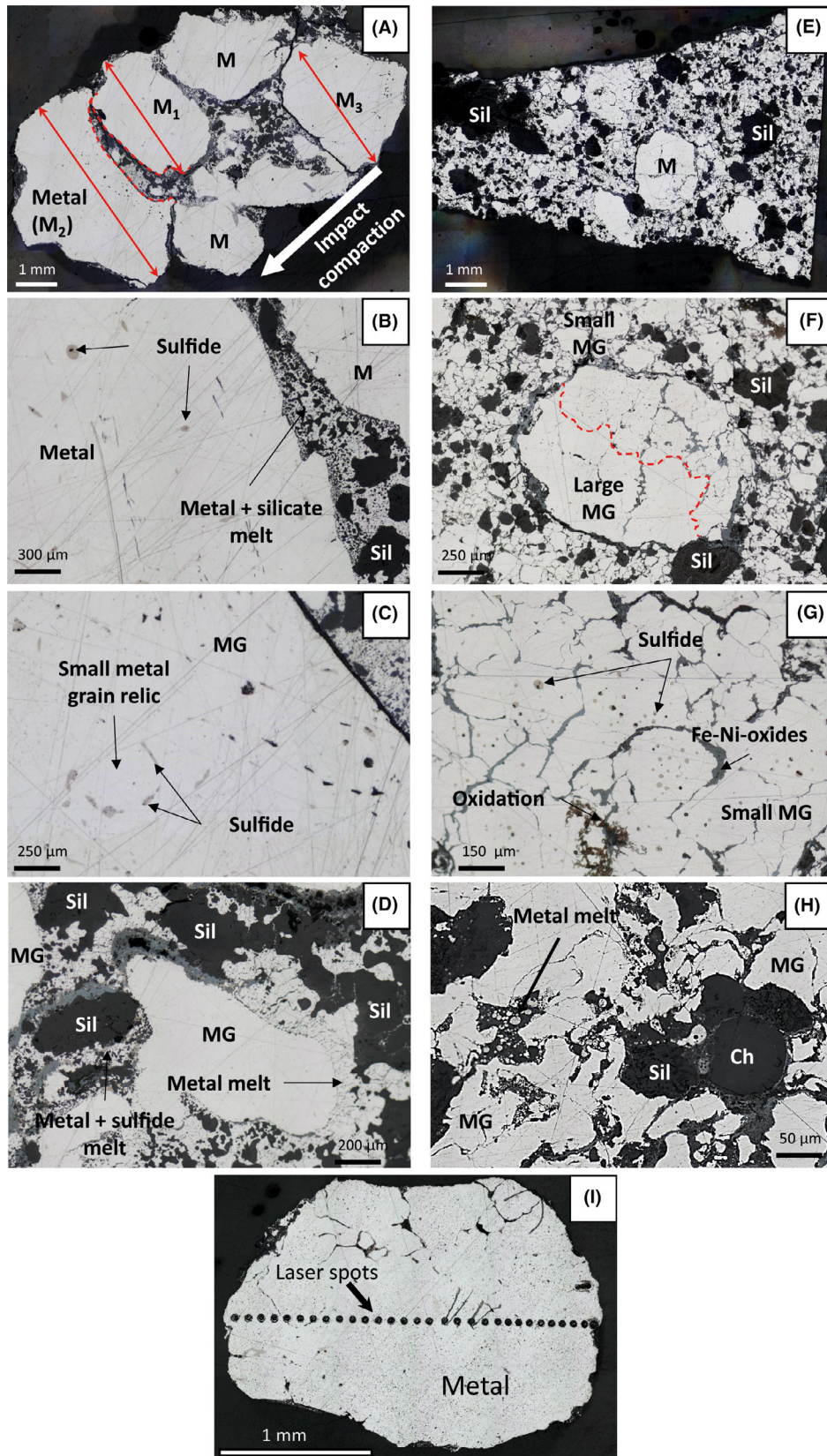


Fig. 1. Reflected-light images of CB_a Bencubbin (A–D) and CB_b HaH 237 (E–H). A) Image detailing the direction of impact compaction in Bencubbin. Red arrows indicate parallel elongation axes in metallic grains M₁, M₂, and M₃, and dashed red lines indicate the footprint of grain M₁ in grain M₂. B) Sulfide inclusions within metal grains and impact melt (mixture of silicates, Sil, with metallic melt) between grains. C) Sulfides delineating a relic of a small metallic grain within a larger one (MG). D) Metal melt formation sourced from the melting of the edges of metallic grains. E) Map of HaH 237 showing the overall texture of silicates (black) and metal (white). F) Comparison of large and small metal grains in HaH 237. The red dashed line divides the central large grain into two zones: a fully aggregated part (bottom left) and a partially aggregated part (top right). G) Enlarged view of the partially aggregated part of the large grain in (F), highlighting the constituent smaller metal grains. H) Immiscible metal and silicate melts formed upon impact. Chondrules (Ch) and chondrule relics are also visible. I) A rounded metal grain from CB_a Gujba, with analytical spots from an LA-ICP-MS profile.

chondrule relics (based on their petrographic shapes) that are sometimes deformed or (2) silicate melt, consistent with the observation of Weisberg et al. (2001). Shock melts (Meibom et al. 2005) composed of finely intertwined metal and immiscible silicates occur between metal grains and chondrules (Fig. 1H).

ANALYTICAL PROCEDURES

Elemental Measurements by LA-ICP-MS

Siderophile and chalcophile trace element concentrations were measured in situ by laser ablation inductively coupled plasma mass spectrometry (LA-ICP-MS) following the protocol developed by Alard et al. (2000) and Mullane et al. (2004). Analyses were performed on an Agilent 7700cx ICP-MS coupled with a Photon Machines Analyte G2 193 nm ArF excimer laser ablation system at Macquarie GeoAnalytical (Macquarie University, Sydney, Australia). Each analysis consisted of an individual static spot measurement: the gas background was measured for 160 s (i.e., laser off), followed by 60 s (=300 laser pulses) of integrated analyzed signal (i.e., laser on) and then 60 s of washout time to avoid any memory effects. The measured isotopes are ⁵⁹Co, ⁶⁰Ni, ⁶³Cu, ⁶⁹Ga, ⁷⁴Ge, ⁷⁵As, ⁹⁵Mo, ¹⁰¹Ru, ¹⁰³Rh, ¹⁰⁶Pd, ¹⁰⁷Ag, ¹²¹Sb, ¹²⁵Te, ¹⁸²W, ¹⁸⁵Re, ¹⁹²Os, ¹⁹³Ir, ¹⁹⁵Pt, ¹⁹⁷Au, ²⁰⁸Pb, and ²⁰⁹Bi, and associated internal LA-ICP-MS errors (%) are 1, 1, 5, 5, 23, 9, 10, 10, 10, 10, 45, 37, 55, 29, 29, 11, 20, 10, 12, 39, and 68, respectively. Most of these elements have typical LA-ICP-MS errors between 0 and 20%, and errors >30% are due to very low elemental concentrations. These elements were selected to cover the entire range of volatility for siderophile elements. Data were corrected and processed using GLITTER™ software (Griffin et al. 2008), which allows for the cleanest part of the time-resolved spectrum to be selected, avoiding inclusion phases. Background values were estimated for each analysis, not interpolated throughout the session. A quenched NiS alloy (PGE-A; Alard et al. 2000; Gilbert et al. 2013) doped with selected chalcophile and siderophile elements was used

as an external calibration standard for all elements except Re, W, Mo, Ni, Ga, and Ge, for which we used FeS1 (Wohlgemuth-Ueberwasser et al. 2007). Furthermore, Filomena (Walker et al. [2008] and references therein), Hoba (IVB iron meteorite), and NIST1158 steel (Campbell et al. 2002; Walker et al. 2008) were systematically analyzed in each session to evaluate data. Average results for these standard materials are consistent with previously published values (Table S1 in supporting information). Detection limits for LA-ICP-MS analyses are calculated as the average background concentrations plus three standard deviations. Typical detection limits obtained during this study and more details of the analytical about LA-ICP-MS settings used are provided in the LA-ICP-MS section and Table S2 of supporting information.

Germanium Isotopic Analyses

Sample Preparation and Digestion

Slices of ≈300 mg of Bencubbin and HaH 237 and two fully preserved spherical metal grains ~2 mm in diameter (157 and 137 mg) separated from Gujba were cleaned with 0.2 M HNO₃ in an ultrasonic bath for 5 min at room temperature to remove external oxidation; any unwanted metal, silicate, sulfide, melt, or matrix clinging to them; and any possible terrestrial contamination. Samples were rinsed with ultrapure Milli-Q water to remove the acid, then with acetone to avoid oxidation, and dried overnight in a laminar-flow hood. High purity SeaStar® acids were used for all cleaning, digestion, and resin separation steps.

Bulk Metal Grains

Bulk metal from Bencubbin and HaH 237 (214 and 230 mg, respectively) were digested overnight in 8 mL of 2 M HNO₃ at 60–65 °C in a Teflon beaker. After full digestion, remaining silicate grains enclosed in the metal were removed by centrifugation and cleaned for 10 min with 2 mL of cold 2 M HNO₃ in an ultrasonic bath to fully recover the digested metal solution. Florin et al. (2020) demonstrated that silicates are not digested using this protocol.

Sequentially Digested Metal Grains

To measure intra-grain Ge elemental and isotopic variations, each of the two metal grains from Gujba was sequentially digested in an ultrasonic bath of 2 M HNO₃ into rim, intermediate, and core fractions. To obtain the rim fraction, digestion was stopped every 20 min and each grain was rinsed with Milli-Q water, dried in acetone, and weighed; this was repeated until ~33% of the mass was digested. The water used to rinse the grains was recovered and added to the solution to avoid losing material. We repeated the same protocol in another beaker until another ~33% of the mass was digested to obtain the intermediate fraction. Finally, the remaining mass (the core fraction) was entirely digested in a third beaker. (Fraction weights will be reported in Table 2.)

Germanium Elemental and Isotopic Measurements by HG-MC-ICP-MS

We adapted the chemistry procedure of Luais (2007, 2012) to a larger metal sample mass to accommodate the low Ge concentrations in CB chondrites (around 1 ppm); further details are given in the supporting information. The Ge elemental and isotopic compositions of sample solutions in 0.5 M HNO₃ were analyzed using a NeptunePlus multicollector inductively coupled plasma mass spectrometer coupled with a hydride generator system (HG-MC-ICP-MS) at the Centre de Recherches Pétrographiques et Géochimiques (Nancy, France; see Rouxel and Luais [2017] and references therein; Florin et al. 2020). ⁶⁸Zn, ⁶⁹Ga, ⁷⁰Ge, ⁷¹Ga, ⁷²Ge, ⁷³Ge, and ⁷⁴Ge were analyzed in static mode on the L3, L2, L1, C, H1, H2, and H3 Faraday cups, respectively. The intensity obtained for the 10 ppb Ge NIST3120a standard solution was 1.8 V on ⁷⁴Ge. Bulk Ge procedural blanks, including chemistry and HG-MC-ICP-MS measurements, were <70 pg (12 mV); as this amount is negligible (corresponding to <0.1% of the chemically processed Ge), no blank corrections were applied. Samples were measured for 320 s, comprising 40 integration cycles of 8 s each, and were bracketed using the NIST3120a Ge standard solution.

Because the chemical yield for Ge metal is 100% (Luais 2007; see appendix C), Ge elemental concentrations were calculated by comparing the Ge intensity on mass 74 measured for each sample with the intensity of the 10 ppb Ge NIST3120a standard for which the concentration is known. Additionally, Ge concentrations were cross validated by measuring Magura (IAB iron meteorite), an in-house standard of the same matrix composition, during the same sessions. We estimate the uncertainty on our measurements to be 8% to account for the precisions of weighing (5%), dilution (1%), and intensity measurements (5%).

Isotopic data are reported using delta notation (δ , ‰) as ^xGe/⁷⁰Ge ratios relative to the mean ratios of the NIST3120a Ge standard analyzed before and after each sample (Luais 2012):

$$\delta^{x/70}\text{Ge} = \left(\frac{(^x\text{Ge}/^{70}\text{Ge})_{\text{sample}}}{(^x\text{Ge}/^{70}\text{Ge})_{\text{NIST3120a}}} - 1 \right) \times 1000 \quad (1)$$

where x indicates the mass number (72, 73, 74) of the analyzed Ge isotope. During each analytical session, JMC and Aldrich Ge standard solutions were analyzed, yielding $\delta^{74/70}\text{Ge} = -0.32 \pm 0.17\text{‰}$ ($n = 16$) and $\delta^{74/70}\text{Ge} = -1.96 \pm 0.12\text{‰}$ ($n = 18$), respectively (2σ SD). The in-house Magura standard yielded $\delta^{74/70}\text{Ge} = 0.80 \pm 0.09\text{‰}$ ($n = 5$). These values are consistent with those reported by Luais (2007, 2012) and Escoube et al. (2012). In general, sample reproducibility on $\delta^{74/70}\text{Ge}$ is better than 0.1‰ (= 0.06 ‰ for Magura; Luais 2007). However, we cannot calculate reproducibilities for samples with very low concentrations that can only be measured once, as was the case for some fractions of the sequentially digested Gujba metal grains. In those cases, the reported $\delta^{x/70}\text{Ge}$ reproducibility is given to be similar to that for the in-house Magura iron meteorite standard measured during the same session.

RESULTS

Elemental Compositions

In Situ Analyses

HSE and MSE contents of metal grains were obtained by LA-ICP-MS in two grains from Gujba, three from HaH 237, and two from Bencubbin. We performed 10–27 aligned static spot analyses across the large grains (Fig. 1I) and three to four aligned static spot analyses in the other grains for a total of 74 spot analyses (average values are reported in Table 1 and Fig. 2; all values are available in Table S3 in supporting information). The mean compositions of our LA-ICP-MS results (Fig. 2) are consistent with previous data on CB chondrites (literature data: [Re]_{mean} ≈ 0.3 ppm, [Os]_{mean} ≈ 3.39 ppm, [Ir]_{mean} ≈ 2.03 ppm, [Ga]_{mean} ≈ 1.89 ppm, [Ge]_{mean} ≈ 0.76 ppm; Campbell et al. 2002, 2005; Weyrauch et al. 2019). Compared to CI chondrites, metal grains are enriched in refractory siderophile elements (e.g., $2 < [\text{Ir}]_{\text{N}} \leq 6$ and $5 < [\text{Pt}]_{\text{N}} < 10$, where the subscript “N” indicates concentrations normalized to those in CI chondrites; CI chondritic values after Lodders et al. 2009). Although elemental variations are observed between and within metal grains, we do not observe any clear HSE or MSE

Table 1. Mean elemental compositions of each grain analyzed (in ppm, Ni in %) as determined by LA-ICP-MS. The mean column refers to the average of all analyses for each meteorite. The full data table is provided in Table S3.

<i>n</i>	Gujba												Bencubbin												HaH 237											
	30				33				10				4				14				18				3				3				24			
	Grain 1	SE	Grain 2	SE	Mean	SE	Grain 1	SE	Grain 2	SE	Mean	SE	Grain 1	SE	Grain 2	SE	Mean	SE	Grain 1	SE	Grain 2	SE	Mean	SE	Grain 1	SE	Grain 2	SE	Mean	SE						
Re	0.12	0.01	0.05	0.01	0.12	0.01	0.10	0.01	0.07	0.01	0.09	0.01	0.39	0.07	0.28	0.02	0.24	0.01	0.39	0.07	0.28	0.02	0.24	0.01	0.39	0.07	0.28	0.02	0.24	0.01	0.35	0.05				
Os	1.43	0.03	1.16	0.02	1.40	0.03	1.12	0.04	1.11	0.04	1.11	0.03	2.87	0.09	2.78	0.07	2.45	0.13	2.87	0.09	2.78	0.07	2.45	0.13	2.87	0.09	2.78	0.07	2.45	0.13	2.81	0.07				
W	0.26	0.02	0.15	0.07	0.25	0.02	0.19	0.02	0.16	0.05	0.18	0.02	0.61	0.04	0.60	0.03	0.56	0.08	0.61	0.04	0.60	0.03	0.56	0.08	0.61	0.04	0.60	0.03	0.56	0.08	0.60	0.03				
Ir	1.58	0.04	1.19	0.10	1.54	0.04	1.33	0.04	1.24	0.08	1.30	0.04	3.21	0.08	2.99	0.06	2.75	0.17	3.21	0.08	2.99	0.06	2.75	0.17	3.21	0.08	2.99	0.06	2.75	0.17	3.13	0.07				
Ru	2.39	0.06	1.98	0.22	2.35	0.06	2.31	0.10	2.03	0.09	2.23	0.08	5.03	0.10	4.79	0.19	4.11	0.03	5.03	0.10	4.79	0.19	4.11	0.03	5.03	0.10	4.79	0.19	4.11	0.03	4.88	0.10				
Mo	3.93	0.11	3.84	0.76	3.92	0.11	4.17	0.22	4.15	0.40	4.16	0.18	9.26	0.24	8.18	0.14	8.35	1.20	9.26	0.24	8.18	0.14	8.35	1.20	9.26	0.24	8.18	0.14	8.35	1.20	9.01	0.23				
Pt	3.23	0.06	2.98	0.14	3.20	0.06	2.78	0.11	3.00	0.02	2.84	0.08	6.47	0.17	6.36	0.25	5.71	0.48	6.47	0.17	6.36	0.25	5.71	0.48	6.47	0.17	6.36	0.25	5.71	0.48	6.36	0.15				
Rh	0.56	0.01	0.47	0.04	0.56	0.01	0.49	0.02	0.47	0.02	0.48	0.01	1.11	0.04	1.04	0.04	0.97	0.04	1.11	0.04	1.04	0.04	0.97	0.04	1.11	0.04	1.04	0.04	0.97	0.04	1.08	0.03				
Ni	6.25	0.05	6.61	0.09	6.28	0.05	6.76	0.06	6.80	0.04	6.77	0.04	6.58	0.10	6.89	0.07	6.96	0.14	6.58	0.10	6.89	0.07	6.96	0.14	6.58	0.10	6.89	0.07	6.96	0.14	6.67	0.08				
Co	4968	81	4427	18	4919	78	3536	15	3462	33	3515	16	4065	40	3779	59	3660	25	4065	40	3779	59	3660	25	4065	40	3779	59	3660	25	3979	44				
Pd	2.18	0.04	1.73	0.23	2.14	0.04	1.96	0.06	2.03	0.17	1.98	0.06	2.12	0.05	2.16	0.09	2.09	0.21	2.12	0.05	2.16	0.09	2.09	0.21	2.12	0.05	2.16	0.09	2.09	0.21	2.12	0.05				
As	4.55	0.09	5.14	0.57	4.60	0.10	2.36	0.14	2.53	0.20	2.41	0.11	2.98	0.14	3.07	0.21	3.03	0.28	2.98	0.14	3.07	0.21	3.03	0.28	2.98	0.14	3.07	0.21	3.03	0.28	3.00	0.11				
Au	0.30	0.01	0.31	0.11	0.30	0.01	0.20	0.02	0.18	0.02	0.19	0.01	0.24	0.01	0.20	0.01	0.26	0.01	0.24	0.01	0.20	0.01	0.26	0.01	0.24	0.01	0.20	0.01	0.26	0.01	0.23	0.01				
Cu	122.64	5.51	68.85	0.90	117.75	5.70	7.66	0.43	6.96	0.27	7.46	0.32	49.46	3.69	40.07	1.13	42.34	2.25	49.46	3.69	40.07	1.13	42.34	2.25	49.46	3.69	40.07	1.13	42.34	2.25	47.39	2.86				
Ag	0.04	0.01	0.04	0.01	0.04	0.01	0.03	-	0.03	0.01	0.03	0.01	0.03	-	B.L.	-	B.L.	-	0.03	-	B.L.	-	B.L.	-	0.03	-	B.L.	-	0.03	0.01	0.03	0.01				
Sb	0.18	0.02	0.36	0.12	0.19	0.02	0.19	0.03	0.08	0.02	0.15	0.02	0.09	0.01	0.11	0.04	0.10	0.02	0.09	0.01	0.11	0.04	0.10	0.02	0.09	0.01	0.11	0.04	0.10	0.02	0.09	0.01				
Ga	3.38	0.06	3.71	1.25	3.40	0.12	0.92	0.05	0.99	0.14	0.94	0.05	1.81	0.04	1.67	0.04	1.59	0.11	1.81	0.04	1.67	0.04	1.59	0.11	1.81	0.04	1.67	0.04	1.59	0.11	1.76	0.04				
Ge	0.86	0.03	1.29	0.06	0.89	0.05	0.34	0.05	0.24	0.06	0.31	0.04	0.54	0.04	0.52	0.05	0.38	0.12	0.54	0.04	0.52	0.05	0.38	0.12	0.54	0.04	0.52	0.05	0.38	0.12	0.52	0.03				
Bi	0.02	0.01	0.02	0.01	0.02	0.01	0.02	0.01	0.01	0.01	0.01	-	0.02	-	B.L.	-	0.01	-	0.02	-	B.L.	-	0.01	-	0.02	-	B.L.	-	0.02	-	0.02	-				
Pb	0.11	0.01	0.19	0.06	0.12	0.01	0.14	0.03	0.47	0.18	0.25	0.06	0.11	0.02	0.23	0.08	0.17	0.07	0.11	0.02	0.23	0.08	0.17	0.07	0.11	0.02	0.23	0.08	0.17	0.07	0.12	0.02				
Te	0.14	0.01	0.24	0.08	0.14	0.01	0.14	0.03	0.09	0.02	0.13	0.02	0.22	0.02	0.12	0.04	B.L.	-	0.22	0.02	0.12	0.04	B.L.	-	0.22	0.02	0.12	0.04	B.L.	-	0.20	0.02				
Co/Ni	0.080	0.002	0.067	0.001	0.078	0.002	0.052	0.001	0.051	0.001	0.052	0.001	0.062	0.001	0.055	0.001	0.053	0.001	0.062	0.001	0.055	0.001	0.053	0.001	0.062	0.001	0.055	0.001	0.060	0.001	0.060	0.001				
W/Mo	0.07	0.01	0.04	0.01	0.06	0.02	0.05	0.01	0.04	0.01	0.04	0.02	0.07	0.01	0.07	0.01	0.07	0.01	0.07	0.01	0.07	0.01	0.07	0.01	0.07	0.01	0.07	0.01	0.07	0.01	0.07	0.01				
Au/Ir	0.19	0.01	0.25	0.06	0.19	0.01	0.15	0.02	0.15	0.01	0.15	0.01	0.07	-	0.07	-	0.09	0.01	0.07	-	0.07	-	0.09	0.01	0.07	-	0.07	-	0.09	0.01	0.07	0.01				
Pd/Ir	1.40	0.04	1.20	0.16	0.91	0.04	1.49	0.05	1.66	0.20	0.89	0.07	0.67	0.02	0.72	0.02	0.77	0.13	0.67	0.02	0.72	0.02	0.77	0.13	0.67	0.02	0.72	0.02	0.77	0.13	0.43	0.02				
Ni/Ru	2.68	0.08	3.43	0.38	2.67	0.09	2.98	0.13	3.38	0.14	3.04	0.11	1.32	0.04	1.44	0.07	1.69	0.02	1.32	0.04	1.44	0.07	1.69	0.02	1.32	0.04	1.44	0.07	1.69	0.02	1.37	0.04				
Ni/Ir	4.03	0.11	5.63	0.45	4.07	0.13	5.14	0.16	5.54	0.34	5.20	0.15	2.07	0.05	2.31	0.02	2.55	0.12	2.07	0.05	2.31	0.02	2.55	0.12	2.07	0.05	2.31	0.02	2.55	0.12	2.13	0.05				

n = the number of spot analyses within each grain; B.L. = below detection limit. Errors are reported as 1 SE.

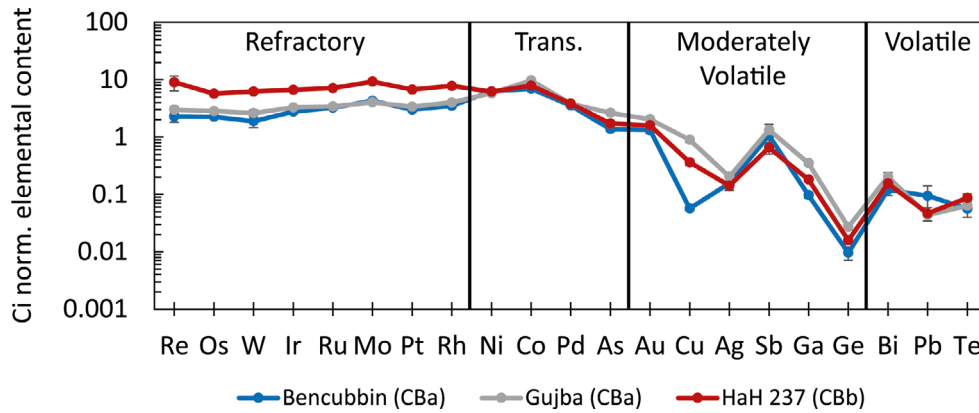


Fig. 2. Mean elemental compositions of the studied CB_a and CB_b meteorites (data in Table 1) based on all LA-ICP-MS spot analyses of each meteorite (data from this study) normalized to CI composition (Lodders et al. 2009). Refractory, transitional, moderately volatile, and volatile refer to the degree of elemental volatility (Walter et al. 2000). Most errors are within the symbol size.

zation in our edge-to-edge analyses, except for Ge (see Germanium concentrations, below). Mo and W contents range from 2.70 ± 0.34 to 11.81 ± 1.12 ppm ($3 < [Mo]_N < 12$) and from 0.04 ± 0.02 to 0.85 ± 0.19 ppm ($10 < [W]_N < 100$), respectively. Re shows slight variations (0.03 ± 0.02 to 0.51 ± 0.09 ppm, $0.76 < [Re]_N < 12.75$), with one higher value in the core of the large HaH 237 grain (1.48 ± 0.24 ppm), and a mean of 0.19 ± 0.32 ppm. Os varies from 0.970 ± 0.16 to 3.79 ± 0.37 ppm ($1.97 < [Os]_N < 7.69$). The Re/Os ratio is chondritic with a median value of 0.095. Ni (5.65 ± 0.10 to 7.18 ± 0.10 wt%, $5.4 < [Ni]_N < 6.5$), Co (0.34 ± 0.01 to 0.56 ± 0.04 wt%, $6.7 < [Co]_N < 11.1$), Pd (1.36 ± 0.18 to 2.73 ± 0.32 ppm, $1.5 < [Pd]_N < 4.2$), As (1.52 ± 0.19 to 6.27 ± 1.33 ppm, $0.9 < [As]_N < 3.5$), and Au (0.12 ± 0.02 to 0.4 ± 0.05 ppm, $1.0 < [Au]_N < 2.6$) are enriched relative to CI chondrites, whereas Ag (0.02 ± 0.01 to 0.05 ± 0.02 ppm, $0.10 < [Ag]_N < 0.13$), Ga (0.65 ± 0.03 to 4.05 ± 0.18 ppm, $0.07 < [Ga]_N < 0.41$), Ge (0.21 ± 0.10 to 1.91 ± 0.66 ppm, $0.01 < [Ge]_N < 0.19$), Bi (-0.06 ± 0.02 ppm, $0.10 < [Bi]_N < 0.30$), Pb (0.04 ± 0.02 to 0.86 ± 0.10 ppm, $0.02 < [Pb]_N < 0.32$), and Te (0.04 ± 0.04 – 0.40 ± 0.14 ppm, $0.02 < [Te]_N < 0.17$) are strongly depleted compared to CI chondrites and refractory HSEs (Fig. 2).

Compared to the mean CB_a composition, metal grains in CB_b HaH 237 are enriched in refractory elements (Re, Os, W, Ir, Ru, Mo, Pt, and Rh) by a factor of about two (2.2, 2.3, 2.6, 2.19, 2.1, 2.2, 2.1, and 2, respectively). In Bencubbin, intra-grain W, Os, Rh, Re, and Ir variations are very limited compared to those of Mo, Pt, and Ru; in HaH 237, intra-grain W, Os, Rh, and Ir variations are limited compared to those of Mo, Pt, Ru, and Re (Fig. 3). The largest intra-grain variations are observed for Mo ($\sim 7.57 \pm 0.74$ to 11.81 ± 1.12 ppm) and Re ($\sim 0.20 \pm 0.05$ to $1.48 \pm$

0.24 ppm) in HaH 237 (Fig. 3). Except for Cu, intra-grain volatile element variations are very limited in all grains, and we did not observe any refractory or volatile element zonings in large metal grains, as expected for condensation from the solar nebular gas (Fig. 3; Fig. S2 in supporting information).

The two groups have similar Ni contents (Bencubbin: 6.7 wt%; Gujba: 6.2 wt%; HaH 237: 6.7 wt%; average: 6.5 wt%) that are five times those in CI chondrites (1.08 wt%; Lodders et al. 2009). The Co/Ni ratios in metal grains of Gujba (0.063 ± 0.019 to 0.100 ± 0.020 SD) and HaH 237 (0.051 ± 0.023 to 0.074 ± 0.02 SD) are high compared to the solar value ($Co/Ni_{solar} = 0.045$; Weisberg et al. 1995, 2001), whereas those in Bencubbin (0.047 ± 0.025 to 0.057 ± 0.025 SD) are more similar to the solar value (Table S3).

Germanium Concentrations

Bulk metal from Bencubbin (CB_a) and HaH 237 (CB_b) display similar Ge concentrations of 0.91 ± 0.07 and 1.34 ± 0.1 ppm (Fig. 4), respectively, consistent with the intra-grain variations observed herein (0.23 ± 0.13 to 1.91 ± 0.66 ppm, Table 1; Fig. S2). The bulk metal Ge contents of each grain from Gujba (CB_a), calculated using the elemental compositions and masses of the rim, intermediate, and core fractions (Fig. 4), show that the two metal grains have mean Ge concentrations of 1.25 ± 0.29 and 0.98 ± 0.16 ppm. These values are similar to previous results on the bulk CB metal (~ 0.9 ppm Ge on average; e.g., Weyrauch et al. 2019), individual metal grains (0.11 ± 0.03 to 1.35 ± 0.02 ppm Ge on average in CB_b ; Campbell et al. 2002; 0.91 ± 0.11 to 1.15 ± 0.14 ppm Ge in Bencubbin; Kallemeyn et al. 1978), and LA-ICP-MS analyses of unzoned (0.23 ± 0.13 to 0.41 ± 0.15 ppm Ge in Bencubbin, 0.58 ± 0.15 to 1.91 ± 0.66 ppm Ge in Gujba, 0.21 ± 0.10 to

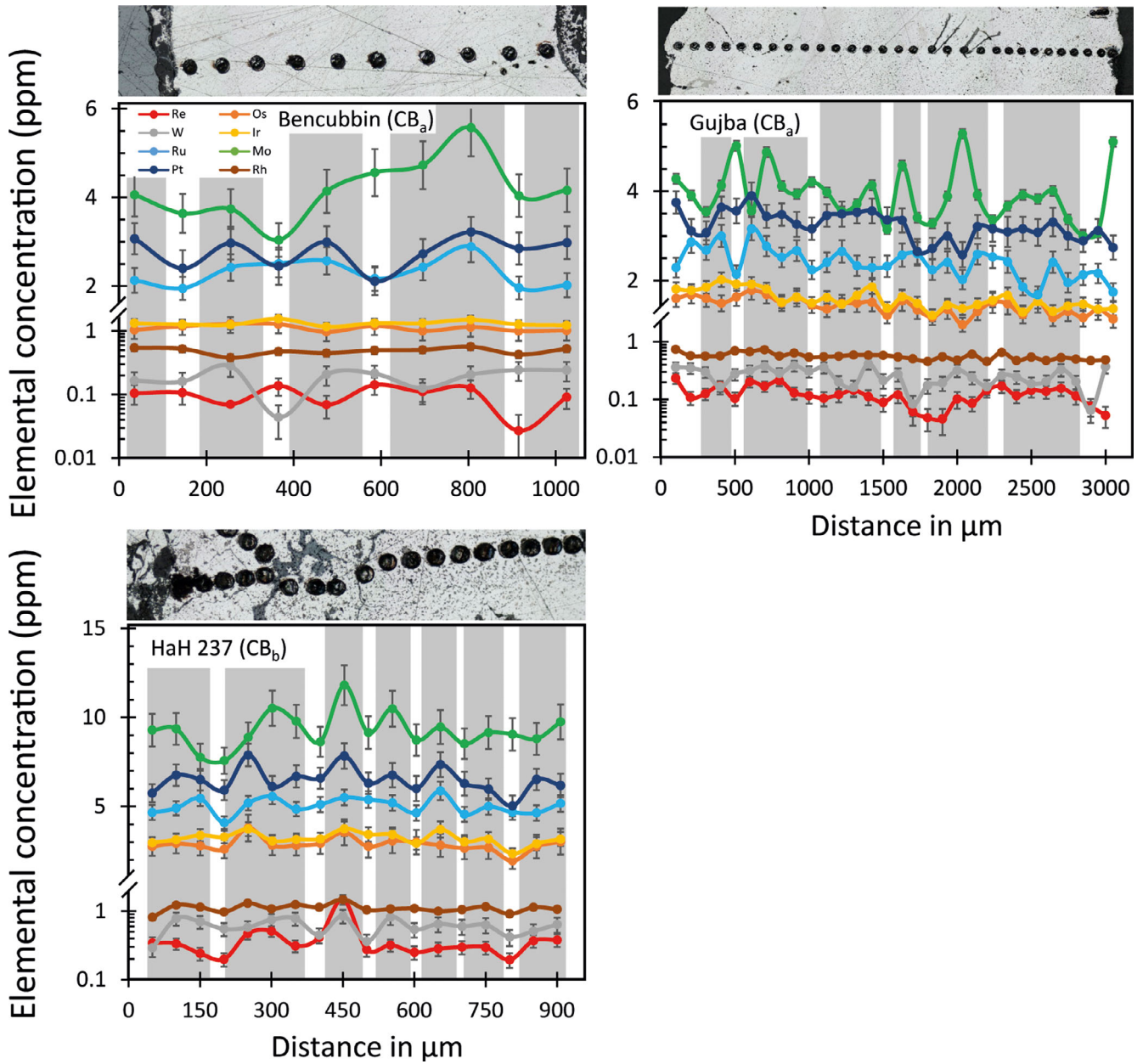


Fig. 3. Cross sections of refractory element content in CB_a and CB_b metal grains. Re, Rh, and W (Gujba and HaH 237) and Re, Rh, W, Ir, and Os (Bencubbin) are plotted on a log scale. Because refractory elements are enriched in earlier condensates, metal grain cores and edges are, respectively, identified based on concentration peaks and relative depletions (mainly Pt, Ru, and Re). Based on these peaks, gray bands highlight potential small grains that aggregated to form the larger ones.

0.84 ± 0.16 ppm Ge in HaH 237; this study) and zoned metal grains (up to 11 ppm Ge in metal in CB_b chondrites, mean 0.9 ppm Ge; Weyrauch et al. 2019). Ge contents in CB metal are up to 30 times lower than those in CI chondrites (33.2 ± 0.3 ppm; Lodders 2003). Ge contents in CB metal grains are also very low compared to most iron meteorite groups (80–180 ppm in magmatic

irons, 60–380 ppm in non-magmatic irons; Wasson 1969; Luais 2007) and metal in ordinary chondrites (H group, ~60 ppm; L group, ~130 ppm; LL group, ~250 ppm; Chou and Cohen 1973; Florin et al. 2020). However, CB metal concentrations are similar to other iron meteorite groups, such as IVA-IVB (~0.03–0.14 ppm; Schaudy et al. 1972), IIIF (~0.7–1.1 ppm; Scott and Wasson

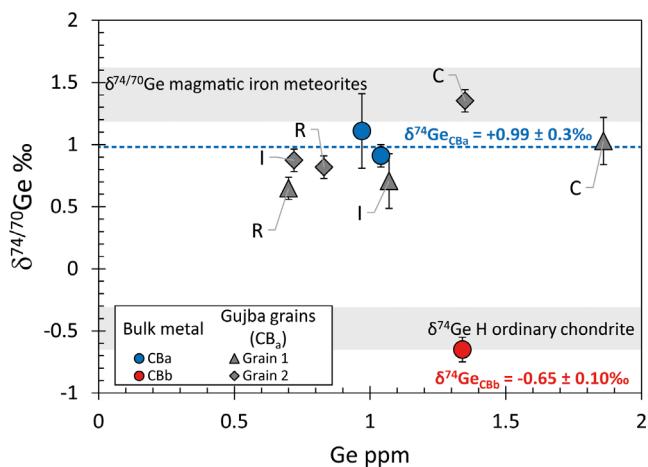


Fig. 4. Germanium contents and isotopic composition of CB chondrites. The mean isotopic values of CB_a metal are positive ($0.99 \pm 0.31\%$) whereas those of CB_b are negative ($-0.65 \pm 0.1\%$). Gujba grain 1 and Gujba grain 2 display the same isotopic zonation, but shifted by a few per mil. Letters refer to Gujba grain fractions: R = rim; I = intermediate; C = core.

1976), and IID (~1.4–4.0 ppm; Wasson and Schaudy 1971).

From rim to core, Ge concentrations in metal grains from Gujba increase from 0.7 ± 0.05 to 1.86 ± 0.14 ppm in grain 1 and from 0.83 ± 0.06 to 1.35 ± 0.1 ppm in grain 2 (Fig. 4, Table 2). Variations within the intermediate fraction are not distinct from the rim fractions, likely due to a mixing between the rim and core fraction during the sequential digestion process. Additionally, due to the low spatial resolution of our analysis, it is impossible to know if the core–rim increase is gradual or abrupt. These values are of the same order of magnitude as those reported for the bulk Gujba metal (1.08 ppm) by Weyrauch et al. (2019), although they did not identify any Ge zonations in metal grains. This may result from the varied thermal histories of different grains (see the Ge diffusion in metal grains section).

Ge Isotopic Compositions

We analyzed the Ge isotopic compositions of bulk metal grains from Bencubbin and HaH 237 and the rim, intermediate, and core fractions of two rounded metal grains from Gujba (reported errors are 2σ SD; Fig. 5). The bulk Ge isotopic compositions of each grain from Gujba were calculated based on the observed values and masses of the rim, intermediate, and core fractions (Table 2). In the $\delta^{72/70}\text{Ge}$ versus $\delta^{74/70}\text{Ge}$ diagram (Fig. S3 in supporting information), all data plot on the mass-dependent fractionation line.

Bencubbin bulk metal has a high $\delta^{74/70}\text{Ge}$ value of $1.04 \pm 0.09\%$ (Table 2), consistent with the calculated bulk metal values of the sequentially digested metal grains from Gujba, $\delta^{74/70}\text{Ge} = 0.81 \pm 0.47\%$ and $1.02 \pm 0.37\%$ (Table 2). Notably, the $\delta^{74/70}\text{Ge}$ values of Bencubbin and Gujba metal are positive, as in magmatic iron meteorites ($\delta^{74/70}\text{Ge} = 1.41 \pm 0.22\%$; Luais 2012) and the metal phases of pallasites ($\delta^{74/70}\text{Ge} = 1.01 \pm 0.04\%$; Luais et al. 2017) values. In comparison, HaH 237 bulk metal has a lighter and, notably, negative $\delta^{74/70}\text{Ge}$ value of $-0.65 \pm 0.1\%$, very close to that of metal in H ordinary chondrites ($\delta^{74/70}\text{Ge} = -0.54 \pm 0.09\%$; Florin et al. 2020).

Gujba metal grains display Ge isotopic zonations that increase from rim to core; the respective $\delta^{74/70}\text{Ge}$ values of the rim, intermediate, and core fractions of grain 1 are $0.65 \pm 0.09\%$, $0.71 \pm 0.22\%$, and $0.99 \pm 0.30\%$, and those of grain 2 are $0.82 \pm 0.09\%$, $0.87 \pm 0.09\%$, and $1.35 \pm 0.09\%$ (Fig. 4; Table 2). Although the rim and intermediate values of grain 1 are indistinguishable, the difference between the rim and core values is beyond analytical reproducibility ($>0.1\%$). Therefore, the observed rim and core increase in $\delta^{74/70}\text{Ge}$ is statistically valid. Finally, the intra-grain Ge isotopic variations contrast the lack of Fe and Ni isotopic zonations observed in Gujba metal grains (Weyrauch et al. 2019).

DISCUSSION

The Formation of Large Metal Grains

Our petrographic observations suggest that large metal grains in CB chondrites are aggregates of smaller ones, in agreement with Weisberg et al. (2001) (Fig. 1). This indicates a two-step formation process, in which small metal grains formed first and then aggregated into larger ones (Weisberg et al. 2001). The textures and sizes of large metal grains in CB_a and CB_b chondrites, as well as the higher degree of homogenization/aggregation of metal grains in CB_a compared to CB_b chondrites (Figs. 1C, 1F, and 1G), suggest that CB_a metal grains experienced prolonged condensation and agglomeration, and thus a longer period at high temperature, than CB_b metal grains, which agglomerated and cooled quickly. In the following we investigate elemental variations in large aggregate metal grains.

The solar Co/Ni ratio varies from 0.037 to 0.054 (calculated from the data of Campbell et al. [2001], using 2σ SD = 0.008), with a mean value of 0.045 (Newsom and Drake 1979; Meibom et al. 1999). Previous studies of smaller metal grains in CB chondrites reported Co/Ni ratios close (within errors) to the mean solar ratio (Newsom and Drake 1979). In

Table 2. Germanium contents and isotopic compositions of bulk metal in CB chondrites and of Gujba grains.

	Ge (ppm)	± (ppm)	$\delta^{72/70}\text{Ge}$ (‰)	2 σ SD	$\delta^{73/70}\text{Ge}$ (‰)	2 σ SD	$\delta^{74/70}\text{Ge}$ (‰)	2 σ SD	% <i>n f</i>
Bencubbin (CB _a)	0.91	0.07	0.58	0.09	0.76	0.25	1.04	0.09	5 –
Gujba (CB _a)	<i>1.11</i>	<i>0.08</i>	<i>0.53</i>	<i>0.12</i>	<i>0.76</i>	<i>0.32</i>	<i>0.97</i>	<i>0.32</i>	– –
HaH 237 (CB _b)	1.34	0.10	−0.29	0.14	−0.59	0.39	−0.65	0.10	3 –
Gujba grain 1									
Core	1.86	0.14	0.43	0.13	0.74	0.49	1.03	0.19	2 38
Intermediate	1.07	0.08	0.37	0.21	0.62	0.61	0.71	0.22	2 28
Rim	0.7	0.05	0.46	0.13	1.07	0.56	0.65	0.09	1 34
Mean	1.25	0.29	0.42	0.11	0.77	0.79	0.86	0.27	– –
Gujba grain 2									
Core	1.35	0.10	0.85	0.13	0.93	0.56	1.35	0.09	1 35
Intermediate	0.72	0.05	0.54	0.13	0.39	0.56	0.87	0.09	1 28
Rim	0.83	0.06	0.51	0.13	0.8	0.56	0.82	0.09	1 37
Mean	0.98	0.16	0.648	0.14	0.736	0.72	1.08	0.16	– –
JMC 10 ppb standard solution	–	–	−0.15	0.1	−0.17	0.35	−0.33	0.08	12 –
Aldrich 10 ppb standard solution	–	–	−0.98	0.1	−1.52	0.57	−1.94	0.08	16 –
Magura (IAB Iron meteorite) in-house standard	–	–	0.37	0.13	0.5	0.56	0.8	0.09	5 –

Errors on Ge contents are 8% (see text for details). % *f* indicates the mass percentage analyzed as edge, middle, or core fractions in the Gujba grains. Means of Gujba grains are calculated from the %*f* and Ge content of each fraction. Gujba bulk metal (values in italics) is recalculated using the mean values of the two measured grains. *n* refers to the number of analysis of each fraction (Gujba grains) or meteorite (Bencubbin and HaH 237). The 2 σ SD values on Ge isotopic compositions for grain fractions with *n* = 1 are taken as the values obtained for Magura (IAB iron meteorite), our in-house standard for extraterrestrial Fe-Ni matrices.

contrast, we measured Co/Ni ratios within large CB metal grains that range from 0.047 to 0.100 ± 0.02 SD (Fig. 5B). Smaller grains composing the larger ones are therefore not representative of all metal condensates under solar nebula conditions, and their compositions must represent either different environments or uncondensed (i.e., inherited) materials compared to those of the larger grains. This suggests that the small metal grains composing the larger ones in Gujba (Co/Ni = 0.063–0.100 ± 0.02 SD) or HaH 237 (Co/Ni = 0.051–0.074 ± 0.02 SD) experienced diverse formation conditions, whereas the narrow range observed in Bencubbin (Co/Ni = 0.047–0.049 ± 0.02 SD) is likely due to their formation in a local area characterized by solar nebular conditions. Newsom and Drake (1979) and Weisberg et al. (1990) reported higher Co/Ni ratios (i.e., ≈ 0.6) associated with high Si contents in the metal (≈ 2.3 wt%) that may reflect a time and/or place characterized by particularly reducing conditions.

The distinct redox-sensitive behaviors of the refractory siderophile elements W and Mo allow us to investigate the redox conditions during metal formation. In environments characterized by high *f*O₂, high temperatures, and high cooling rates, W occurs as WO₃, whereas Mo occurs in its metallic form in the gas (Fegley and Palme 1985). Metal grains that condensed under “oxidizing conditions” (nb: above the W-WO₃ or W-WO₂ buffers, 2–4 log units below the iron–wüstite

buffer) should therefore be more depleted in W than in Mo (Fegley and Palme 1985), as observed in both CB_a and CB_b chondrites. The fact that CB_a metal is even more depleted in Mo and/or W than CB_b metal (Fig. 5A) indicates that CB_a metal may have formed in a more oxidizing environment or have been exposed to high temperature for a longer period of time than most CB_b metal. The difference between our CB_b data in Fig. 5A and the low and constant W contents in metal reported in the literature (Campbell et al. 2002; Weyrauch et al. 2019) can be attributed to higher cooling rates, as demonstrated in the next paragraph for Au/Ir data. Additionally, our W/Mo ratios and most previously reported data (e.g., Campbell et al. 2002; Weyrauch et al. 2019) lie below the W/Mo solar value (Fig. 5B), indicative of redox states more oxidizing than in the protoplanetary disk. Because Ni becomes increasingly enriched in Fe-Ni metal with increasing oxidation state (Luais 2007), the large W/Mo variations (0.02 ± 0.15 – 0.10 ± 0.33 , Fig. 5B) and narrow Co/Ni variations (~ 0.05) in Bencubbin preclude any link between the Co/Ni variations in CB_a and CB_b metal, and thus any changes in oxidation state in the environment of CB formation. This lack of variation can be linked to conditions more reduced than the Ni-NiO buffer, as suggested by the occurrence of Si in some metal grains (Weisberg et al. 1990). HSE and MSE variations in large metal grains can reflect the

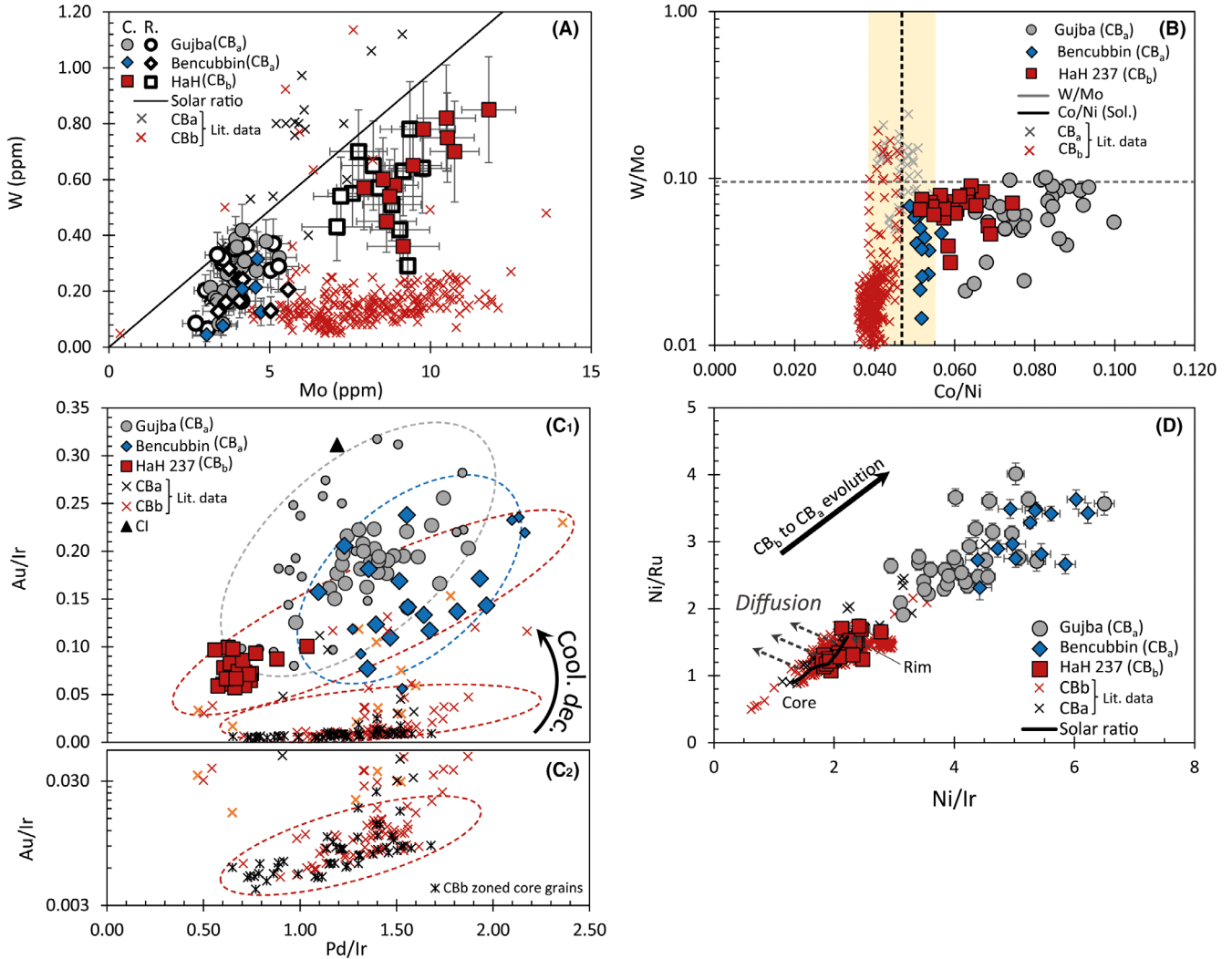


Fig. 5. A) W versus Mo diagram; open symbols indicate grain rim (R) and closed symbols grain cores (C). B) W/Mo versus Co/Ni ratios. The two dashed lines represent CI ratios. The yellow shaded area is the range of variation of the solar Co/Ni ratio, calculated as the 2σ SD range of the data from Campbell et al. (2002). (C₁) Au/Ir versus Pd/Ir ratios. Metal grains do not have CI values (Lodders et al. 2009). Gray (Gujba), blue (Bencubbin), and red (HaH 237) ellipses represent the range of variations for each meteorite. The arrow at bottom right indicates decreasing cooling rate. Small symbol for Gujba and Bencubbin represent literature data (C₂) Low-Au/Ir values plotted on a log scale to show detail. D) Ni/Ru versus Ni/Ir ratios. The dark line represents the evolution of the solar nebular composition of the metal from the core to the rim of condensate metal grains. The dashed arrows show the expected compositional variations due to diffusion (from the data of Righter et al. 2005). Note that these particular CBa grains do not have solar values. CB_a (Campbell et al. 2002) and CB_b (Weyrauch et al. 2019) literature data are shown as gray (CB_a grains), red (zoned CB_b grains), black (core of zoned CB_b grains) and orange (unzoned CB_b grains) crosses.

formation conditions of CB chondrites, particularly the influence of temperature on condensation (Ir, Au, and Pd) and diffusion (Ir, Ru, Ni, and Co; Righter et al. 2005). The Au/Ir and Pd/Ir elemental ratios of our samples (which vary from 0.06 ± 0.22 to 0.32 ± 0.27 and from 0.56 ± 0.30 to 1.96 ± 0.26 , respectively) of our samples define two populations of metal grains that lie on a continuous trend (Fig. 5C). Because of the different volatilities of these elements (Wood et al. 2019), this suggests that CB_a and CB_b metals represent

a continuum between two environments. If metal in the two analyzed CB_a chondrites and in HaH 237 (CB_b) condensed from the same gas, the increasing volatility from Ir ($T_{50} = 1603$ K) to Pd ($T_{50} = 1324$ K) to Au ($T_{50} = 1060$ K) implies that earlier condensates would have higher Ir contents than later ones. Hence, the higher Au/Ir and Pd/Ir ratios of CB_a compared to CB_b (Fig. 5C) imply that metal in Bencubbin and Gujba formed later than that in HaH 237. In addition, comparison with literature data (61 analyzed grains)

confirms the two main trends in Au/Ir–Pd/Ir space (Fig. 5C). These include (1) CB_b grains with constant Au/Ir and variable Pd/Ir (zoned grains) and (2) CB_a and some CB_b grains with constant Au/Ir positively correlated with Pd/Ir (mostly unzoned grains). Based on the differences in T_{50} between Ir, Pd, and Au, these trends can be interpreted in terms of cooling dynamics, with higher slopes indicating slower cooling rates. Hence, the low, relatively constant Au/Ir values in zoned CB_b grains associated with large Pd/Ir variations (Fig. 5C2) reflect condensation at high temperature followed by fast cooling at a low temperature, similar to $T_{50\%}(\text{Pd})$, inhibiting extensive Au incorporation in these metal grains. In contrast, the correlated Au/Ir and Pd/Ir variations in unzoned CB_a and CB_b grains (Fig. 5C1) indicate condensation over a larger range of temperatures and slower cooling, with CB_a cooling the slowest. In this dataspace, data plotting between the two CB_b trends (Fig. 5C1) reflects a mix of unzoned and zoned grains, likely indicating an evolution from fast to slow cooling rates. Therefore, HaH 237 metal grains, and more broadly CB_b grains, formed earlier and more rapidly than Bencubbin and Gujba (CB_a) grains, consistent with the increased occurrence of large aggregate metal grains in CB_a compared with CB_b chondrites.

If the differences between metal grains in CB_a and CB_b chondrites are linked to the duration of their formation at high temperature, the well-agglomerated CB_a grains represent the last step of large metal grain formation. The nonsolar Ni/Ru and Ni/Ir ratios of large CB_a metal grains (Fig. 5D) can therefore be explained by the partial homogenization of most of the refractory elements in the agglomerated small grains during heating events. Because the condensation temperature of Ru is similar to that of Ir but well above that of Ni ($T_{50} = 1551, 1603, \text{ and } 1353 \text{ K}$, respectively, in solar nebular conditions; Lodders et al. 2009), Ru and Ir concentrations should have undergone the same homogenization event that produced the large metal grains. However, based on the diffusivities of Ru, Ni, and Ir in Fe–Ni metal (Richter et al. 2005), a negative Ni/Ru versus Ni/Ir correlation is expected from CB_b to CB_a , whereas we observe a positive correlation (Fig. 5D). This lack of evolution by diffusion is consistent with the HaH 237 Co/Ni ratios (0.051–0.074) that overlap those of both Bencubbin and Gujba (Fig. 5B). As CB_b metal grains must have spent less time at high temperature than CB_a ones, these results suggest that the difference in Co/Ni values between meteorites is not linked to elemental diffusion through small metal grains. Consequently, the small grains must have aggregated into larger ones at temperatures low enough to inhibit the diffusion of refractory elements,

but high enough to seal small grains together, i.e., ~1250–1150 °C, and the elemental compositions of small grains likely result from the prevailing gas pressure or oxidation state at the time of condensation.

These observations suggest that metal in CB chondrites formed as small metal grains that condensed at various gas pressures and cooling rates, then aggregated into larger grains under slow (CB_a) or fast (CB_b) cooling rates. The large compositional variations observed among small grains composing large ones suggest a turbulent and heterogeneous environment that evolved quickly.

Cooling Rates and Ge Isotopic Fractionation during CB_a and CB_b Metal Formation

Richter (2004) showed that the isotopic composition of a solid condensed from a gas mainly depends on cooling rate. Under slow cooling rates, condensing solids reach isotopic equilibrium with the gas and acquire an identical isotopic composition to that of the gas, whereas condensing solids become increasingly isotopically light with increasing cooling rate. If CB_a and CB_b chondrites were formed by condensation from the same gas (as suggested by their common features; Weisberg et al. 2001), the relatively heavy isotopic compositions of the bulk metal in the two CB_a chondrites ($\delta^{74/70}\text{Ge} = 1.04 \pm 0.09\text{‰}$ and $0.92 \pm 0.2\text{‰}$) compared to HaH 237 (CB_b) metal ($\delta^{74/70}\text{Ge} = -0.65 \pm 0.1\text{‰}$, Fig. 4) would imply a slower cooling rate for CB_a metal grains than for CB_b . We note that this observation must be considered with caution as only one CB_b was analyzed, and should be confirmed by studying future newly discovered CB_b chondrites with more available mass. Nevertheless, based on analyzed samples, the $\delta^{74/70}\text{Ge}$ values of the bulk CB_a metal suggest protracted condensation in a hot environment, allowing the metal to record a heavy composition similar to that of the gas, whereas the light $\delta^{74/70}\text{Ge}$ values of the bulk CB_b metal suggest a faster cooling rate, consistent with petrographic observations.

To estimate CB_a and CB_b cooling and growth rates, we updated the method of Meibom et al. (2000) with the most recent values of the total pressure of CB formation (i.e., $P^{\text{tot}} = 10^{-3}$ – 10^{-2} bar; Fedkin et al. 2015) and the Fe condensation temperature ($T_{50} = 1338 \text{ K}$; Wood et al. 2019). The growth rate model calculation is based on the assumptions (1) that growing particles are spherical and composed of 100% of Fe, and (2) that each atom colliding with a metal particle sticks to its surface, obtained growth rates are thus probably slightly overestimated. Nonetheless, under these conditions, we found that increasing P^{tot} from 10^{-4} to 10^{-3} or 10^{-2} bar dramatically increases the growth rate of metal grains

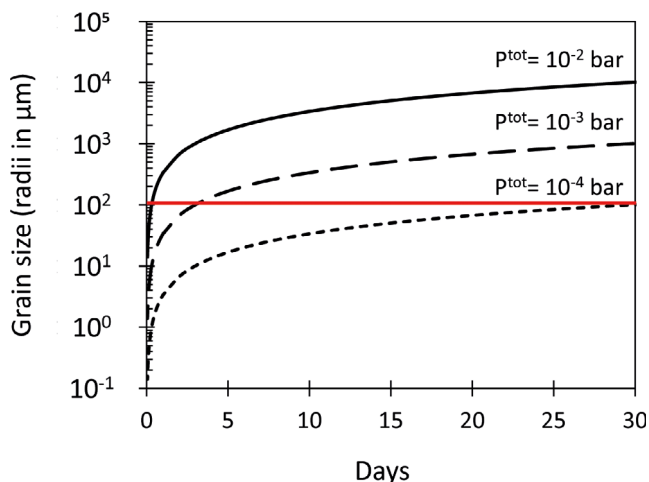


Fig. 6. Growth rates of metal grains at various gas pressures: solid curve, 0.14 $\mu\text{m}/\text{h}$; long-dashed curve, 1.40 $\mu\text{m}/\text{h}$; small-dashed curve, 14.08 $\mu\text{m}/\text{h}$. The red line represents a grain of 100 μm , typical of the grain size observed in the CB meteorites investigated herein. Growth rate calculations are based on the model of Meibom et al. (2000).

from 0.14 to 1.40 to 14.08 $\mu\text{m h}^{-1}$, respectively (Fig. 6). Only 7 h (at 10^{-2} bar) to 3 days (at 10^{-3} bar) are required for a metallic grain 100 μm in radius to condense under these conditions. Fedkin et al. (2015) suggested that the parental CB_b gas was less dense than that of CB_a (10^{-3} and 10^{-2} bar, respectively). The condensation of a 100 μm radius CB_b metal grain in 3 days, during which the temperature decreased from ~ 1370 to ~ 1270 K (corresponding to the temperature range required for Fe to fully condense at equilibrium; Wood et al. 2019), represents a maximum CB_b cooling rate of ~ 1 K h^{-1} . According to Meibom et al. (2000), the homogenization of Fe and Ni contents by solid diffusion within 25 μm metal grains requires 100 days and 2 yr at 1300 and 1200 K, respectively. This implies that the ratio between the characteristic condensation and cooling time scales was very small (Richter 2004), consistent with the very low $\delta^{74/70}\text{Ge}$ values observed in CB_b metal. Furthermore, the growth rate of CB_a metal grains at 10^{-2} bar (Fedkin et al. 2015) would have been one order of magnitude faster than that of CB_b metal grains. Nonetheless, given their slow cooling rate and textural homogenization, they must have remained at high temperature for at least 400 days. Thus, CB_a metal grains likely experienced a maximum cooling rate of ~ 0.01 K h^{-1} , slow enough to acquire the heavy $\delta^{74/70}\text{Ge}$ signature of their parental gas.

The Origin of Ge Zonations in Gujba (CB_a) Metal Grains

The cores of the analyzed Gujba metal grains have higher Ge contents and are enriched in heavy Ge

isotopes (1.86 ± 0.14 ppm Ge and $\delta^{74/70}\text{Ge} = 1.03 \pm 0.19\text{‰}$ in grain 1; $\delta^{74/70}\text{Ge} = 1.35 \pm 0.09\text{‰}$ and 1.35 ± 0.10 ppm Ge in grain 2) compared to their rims (0.70 ± 0.05 ppm Ge and $\delta^{74/70}\text{Ge} = 0.65 \pm 0.09\text{‰}$ in grain 1; 0.83 ± 0.06 ppm Ge and $\delta^{74/70}\text{Ge} = 0.82 \pm 0.09\text{‰}$ in grain 2). Although variations in the intermediate fraction are not resolvable (see the Elemental Compositions section), the most important point, discussed in the following, is the increase in [Ge] and $\delta^{74/70}\text{Ge}$ from rim to core. In comparison, Fe and Ni do not show isotopic zonations in most CB_a metal grains with inter-grain isotopic compositions varying from $\delta^{56}\text{Fe} = -0.6$ to 0.61 ‰ and from $\delta^{62}\text{Ni} = 0.56$ to 1.23 ‰ (Weyrauch et al. 2019). As Ge is more volatile than Fe and Ni ($T_{50} = 830$, 1338, and 1363 K, respectively; Wood et al. 2019), its elemental and isotopic zonations in the metal phase likely reflect processes occurring at lower temperatures. Therefore, the observed Ge zonations may suggest that (1) Ge diffused outward from grain cores during one or several heating events; (2) CB_a grains formed close to equilibrium, and thus the outward decreasing $\delta^{74/70}\text{Ge}$ values may indicate an early stage of condensation (see fig. 7 in Richter 2004); or (3) the starting material was isotopically heterogeneous. We explore these three possibilities in the following subsections.

Ge Diffusion in Metal Grains

Because diffusivity increases with increasing temperature, and because light isotopes diffuse faster than heavier ones (Richter et al. 2009), it is tempting to attribute the $\delta^{74/70}\text{Ge}$ zonations observed in CB_a metal grains to isotopic diffusion. Indeed, in a closed system, diffusion would homogenize the Ge contents within grains. However, partial Ge evaporation from grain rims in an open system depletes grain rims in Ge relative to their cores, consistent with our results (see Figs. 4 and 8). Experiments using Ge radioisotopes with very short half-lives (< 10 days) show that Ge self-diffusion is a very slow process (Vogel et al. 1983) because the heavy and light isotopes have very similar diffusivities (e.g., 1.447×10^{-4} $\mu\text{m}^2 \text{s}^{-1}$ for ^{77}Ge and 1.462×10^{-4} $\mu\text{m}^2 \text{s}^{-1}$ for ^{71}Ge , at 900 $^\circ\text{C}$; Campbell 1975), precluding large diffusive isotopic fractionations. Thus, such small diffusive isotopic fractionations cannot account for the significant $\delta^{74/70}\text{Ge}$ zonations in Gujba metal grains.

Near-Equilibrium Kinetic Condensation

At cooling rates substantially faster than those required for equilibrium condensation, the very first condensates should have isotopic compositions similar to that of their source (see fig. 7 in Richter 2004),

producing grain cores that are isotopically heavier than the surrounding (later condensed) parts of the grain. In this case, the isotopically heavier cores would represent <5% of the condensate (Richter 2004), and thus be very difficult to measure. Nonetheless, at slow cooling rates (i.e., closer to equilibrium), an outward decrease in isotopic value of similar magnitude would represent up to 20% of the condensate, then be followed by a strong increase in $\delta^{74/70}\text{Ge}$ values toward the rim, termed here a “wave pattern.” However, the $\delta^{74/70}\text{Ge}$ values of the two studied Gujba metal grains decrease from core to rim (Fig. 7), indicating that either (1) the observed variations from the highest (grain cores) to lowest $\delta^{74/70}\text{Ge}$ and [Ge] values (grain rims) represent only <20% of the total quantity of condensed Ge, or (2) the resolution of our dissolution technique is too coarse to capture the full isotopic wave pattern. If the observed Ge zonations are indeed the result of near-equilibrium kinetic condensation, they must represent only the first steps of Ge condensation (Richter 2004). This implies that the temperature at the end of the formation of the studied Gujba grains was higher than $T_{50}(\text{Ge}) = 830 \text{ K}$ and that the isotopic composition of the parental gas was $\delta^{74/70}\text{Ge} \geq 1.35\text{‰}$, which contrasts with the Bencubbin $\delta^{74/70}\text{Ge}$ value. Furthermore, the aggregation of small grains into larger ones implies the existence of at least two generations of metal grains. The first generation may thus have had heavy $\delta^{74/70}\text{Ge}$ values and agglomerated to form grain cores, whereas the later generation(s) with lighter $\delta^{74/70}\text{Ge}$ values were agglomerated around the cores to form grain rims.

Heterogeneous $\delta^{74/70}\text{Ge}$ Composition of the Gas Source from Successive Condensation and Evaporation Processes

Condensation and evaporation can result in elemental and isotopic fractionations between solids and gases, leading to heterogeneity in the source. Forming metal grains should record such heterogeneities as chemical and isotopic zonations.

To test this, we numerically modeled evaporation and condensation based on Rayleigh fractionation laws. Solid metals condensing from a gas at near-equilibrium conditions acquire bulk elemental and isotopic compositions similar to those of the gas. The isotopic composition acquired during the first step of metal formation represents only 10–20% of the bulk Ge content of the gas (Ge_{gas}) (Richter 2004), leaving the 80–90% of the initial Ge in the gas. If the metal in CB_a chondrites condensed at a slow cooling rate, as suggested by our textural and elemental data for Bencubbin, we would expect that little to no isotopic fractionation occurred between the first condensate and the gas. The bulk metal $\delta^{74/70}\text{Ge}$ value of Bencubbin metal

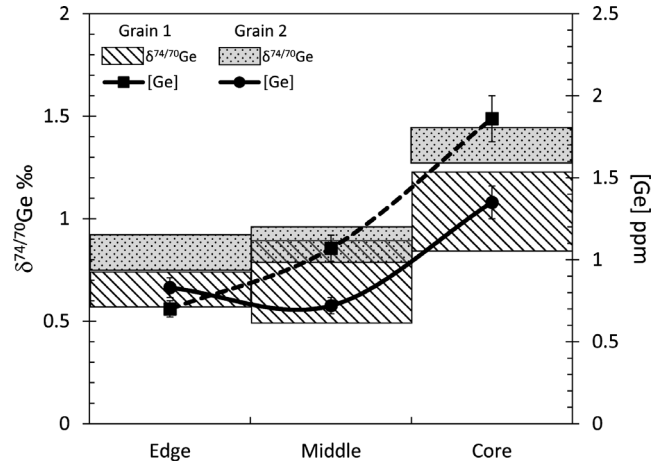


Fig. 7. The core–rim evolution of [Ge] and $\delta^{74/70}\text{Ge}$ zonations in sequentially dissolved CB_a Gujba grains. Squares and curves indicate isotopic compositions, elemental concentrations, respectively, and their 2-SD reproducibilities. The isotopic compositions of the rims and intermediate parts of the two grains overlap. See Table 1 for percentage of each fraction.

($1.04 \pm 0.09\text{‰}$) must then be very close to the isotopic composition of the gas source. It follows that grain cores with $\delta^{74/70}\text{Ge}$ values similar to that of the Bencubbin bulk metal (i.e., the core of grain 1, $\delta^{74/70}\text{Ge} = 1.03 \pm 0.19\text{‰}$) also condensed under slow cooling rates, whereas those depleted in Ge and enriched in heavy isotopes compared to the Bencubbin bulk metal (i.e., the core of grain 2, $\delta^{74/70}\text{Ge} = 1.35 \pm 0.20\text{‰}$) must have experienced evaporation (Fig. 4).

The depletion of Ge in the core of grain 2 ($\text{Ge} = 1.35 \pm 0.10 \text{ ppm}$) compared to the core of grain 1 ($\text{Ge} = 1.86 \pm 0.14 \text{ ppm}$) is reproduced by $\approx 25\%$ Ge evaporation:

$$\%[\text{Ge}]_{\text{evap}} = 1 - \frac{[\text{Ge}]_{\text{core2}}}{[\text{Ge}]_{\text{core1}}} \times 100 \quad (2)$$

where $[\text{Ge}]_{\text{core1}}$ and $[\text{Ge}]_{\text{core2}}$ are the Ge contents of the cores of grains 1 and 2, respectively, and $\%[\text{Ge}]_{\text{evap}}$ is the percentage of evaporation needed to decrease the Ge content from that in the core of grain 1 to that in the core of grain 2.

To quantify evaporation, we assume that small CB_a grains (to later become grain cores) first condensed at a slow cooling rate with $\delta^{74/70}\text{Ge} \approx 1.04 \pm 0.09\text{‰}$. They were then transported to a warmer environment where they quickly reached higher temperatures and experienced partial evaporation. In this scenario, the characteristic time scale of evaporation is smaller to that of heating, not only the enriching of heavy isotopes in the solid relative to the parental gas (Richter 2004), but also

resulting in the formation of plesitic textures in some grains, as observed by Weyrauch et al. (2019). The effect of evaporation on $\delta^{74/70}\text{Ge}$ can be modeled as:

$$\delta^{74}\text{Ge}_f = \left[(1000 + \delta^{74}\text{Ge}_0) \times f^{(\alpha-1)} \right] - 1000 \quad (3)$$

where $\delta^{74}\text{Ge}_f$ is the isotopic composition of the solid after evaporation, $\delta^{74}\text{Ge}_0$ the initial isotopic composition of solids formed at a slow cooling rate (taken as $\delta^{74/70}\text{Ge}_0 = 1.04 \pm 0.09\text{‰}$), f the remaining fraction of Ge in the solid after evaporation, and α the fractionation factor equal to $(m^{70}/m^{74})^\beta$ where m^{70} and m^{74} are the masses of ^{70}Ge and ^{74}Ge , respectively, and β is an empirical parameter that is equal to 0.5 in the case of pure Rayleigh fractionation (here $\beta = 0.03$).

As light isotopes evaporated from this first generation of small metal grains, the gas became enriched in light isotopes and the grains in heavy isotopes. The evolution of the isotopic composition of the gas ($\delta^{74}\text{Ge}_{\text{gas}}$) is calculated as a mixture of the initial gas composition with that of the accumulated vapor produced by Ge evaporation from the metal grains ($\delta^{74}\text{Ge}_{\text{cv}}$) as:

$$\delta^{74}\text{Ge}_{\text{cv}} = \left[(1000 + \delta^{74}\text{Ge}_0) \times \left(\frac{1-f^\alpha}{1-f} \right) \right] - 1000 \quad (4)$$

$$\delta^{74}\text{Ge}_{\text{gas}} = (\delta^{74}\text{Ge}_0 \times f) + \delta^{74}\text{Ge}_{\text{cv}} \times (1-f) \quad (5)$$

Our model results are presented in Fig. 8. Due to the constant arrival of metallic droplets and their partial evaporation, the gas in these warmer regions would have been progressively enriched in light Ge isotopes. Furthermore, as dust pressure increases with increasing temperature, and due to the fast condensation of Fe and Ni (see the Cooling Rates and Ge Isotopic Fractionation during CB_a and CB_b Metal Formation section), earlier generations of metallic grains would have acted as nuclei for the aggregation of later generations of smaller metal grains, which recondensed at equilibrium and insulated their cores, preventing the complete loss of Ge. As the gas cooled, further Ge recondensation at a slow cooling rate recorded the isotopic variations of the gas composition. This second step of condensation may be responsible for the lighter Ge isotopic compositions of the outer parts of metal grains compared to their cores.

The differences between the bulk Ge isotopic compositions of grains 1 and 2 can be explained by a difference in the time of their arrival in the warmer region.

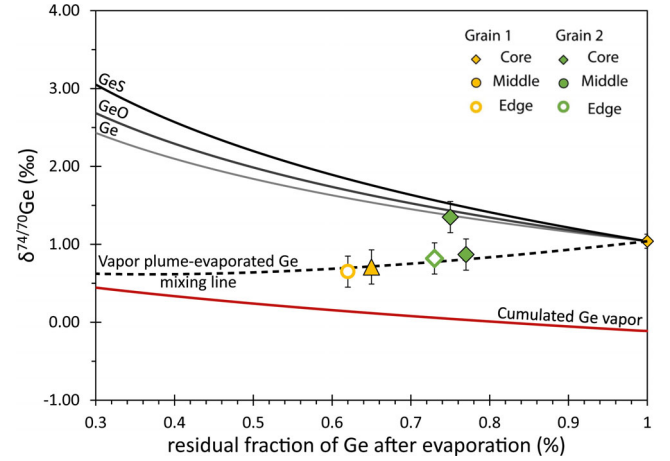


Fig. 8. Rayleigh modeling of $\delta^{74/70}\text{Ge}$ and the percentage of Ge remaining in the metal grain during evaporation. Black, gray, and light gray solid curves show the isotopic evolution of the solid fraction of different Ge species (Ge, GeO, and GeS, respectively) during evaporation with gas-melt isotopic fractionation factors $\alpha = 0.99833$, 0.99864 , and 0.99885 , respectively, defined as $(m^{70}/m^{74})^\beta$ with $\beta = 0.03$. The red line corresponds to accumulated vapor, and the dashed line represents the evolution of the plume gas during mixing with the accumulated vapor. The starting isotopic composition (similar to the plume, see text) and elemental concentration (1.40 ppm, see text) are taken as those of the core of Gujba grain 1. This model demonstrates that the observed zonations in the Gujba metal grains can be explained by mixing of the evaporated Ge with the gas from the plume.

As the gas cooled, grains that arrived earlier in the warmer region (here, the core of grain 2) would have experienced higher temperatures, and thus stronger evaporation and greater enrichment in heavy isotopes, than later-arriving grains (here, the core of grain 1). Grains that arrived near the end of Ge condensation would not have experienced such high temperatures, and therefore would have maintained their inherited equilibrium compositions in their cores. Furthermore, as the gas became progressively isotopically lighter via the cumulative evaporation of previous generations of grains, it would have imparted later-arriving grains with a bulk metal composition isotopically lighter than $\delta^{74/70}\text{Ge} = 1.04 \pm 0.09\text{‰}$. This suggests that grain 1 formed later than grain 2.

Therefore, we conclude that (1) the Gujba (CB_a) metal grain population results from several grain generations; (2) some grains experienced reheating; (3) the isotopic zonations of Gujba metal grains can result from either near-equilibrium condensation or, more likely, a combination of condensation at low cooling rates followed by kinetic evaporation and recondensation, again at low cooling rates; and (4) these processes are not recorded by Fe or Ni isotopes because they occurred at temperatures well below that of Fe-Ni condensation.

DISK VERSUS PLUME MODEL FOR CB METAL FORMATION

Two models have been proposed for the formation of CB chondrites: metal formation by migration in the protoplanetary disk (Meibom et al. 2000) and metal formation in an impact plume (Kallemeyn et al. 2001; Campbell et al. 2002; Rubin et al. 2003; Weyrauch et al. 2019). The elemental compositions of small metal grains suggest that the formation of the Bencubbin and Gujba (CB_a) metals requires at least two different environments. Furthermore, the difference between the Ge isotopic compositions of the analyzed CB_a and CB_b metals requires either a thermally zoned environment, as required to form the Ge isotopic zonations in Gujba (CB_a) metal grains, or two different environments. If CB_a and CB_b metal grains formed distinct locations within the disk, they are likely to have been relatively distant due to the thermal gradient, as supported by the large difference between their $\delta^{74/70}\text{Ge}$ compositions. However, their similar petrological, chemical, and age features suggest that they formed in close proximity to one another. This contradiction can be reconciled by the model of disk-scale convection cells as proposed by Meibom et al. (2000). Although this hypothesis is difficult to test, it raises the question of the uniqueness of CB_a and CB_b chondrites in terms of the elemental and isotopic zonations in their small metal grains. To our knowledge, these specific patterns of condensation in CB metal grains have not been described in the metal components of other chondrites, likely because of their reprocessing by complex heating–cooling cycles (e.g., Okabayashi et al. 2019) in the hot protoplanetary disk. Additionally, CB_a and CB_b components (metal and silicates) formed in a short period of time (4562.2 ± 2.4 Ma Hf-W, Kleine et al. 2005; 4562.49 ± 0.21 Ma Pb-Pb, Bollard et al. 2015); only I-Xe age of HaH 237 (Gilmour et al. 2009; Pravdivtseva et al. 2014) is 1.48 ± 0.9 Myr younger, attributable to inhomogeneous $^{129}\text{I}/^{127}\text{I}$ ratios within the formation environment (Bollard et al. 2015).

Based on these chemical and temporal constraints, we suggest that CB metal formation required a small environment with a steep local thermal gradient: an impact plume. Such a plume must have been thermally zoned, with a steep thermal gradient along its edges and an interior that remained warm for an extended period of time. If CB_a and CB_b metals condensed from the same gas, the higher Au/Ir and Pd/Ir ratios of CB_a compared to CB_b (Fig. 5C) imply that CB_a metal condensed after CB_b metal because Au and Pd are more volatile than Ir. Indeed, CB_b metal is enriched in W and Mo relative to CB_a . Furthermore, because the Au/Ir ratios of metal in Gujba metal are less than that in

Bencubbin, despite their similar Pd/Ir ratios, and because Au is more volatile than Pd, Gujba must have formed after Bencubbin. Given these arguments, CB_a metal must have condensed under slow cooling rates during fewer than 400 days in the inner part of the plume, whereas CB_b metal condensed under fast cooling rates in a few hours to days in the outer part of the plume. Although our conclusions on the formation of CB chondrites are based only on the condensation–evaporation processes linked to the metal phase, the consistency between the Hf-W ages of metal and the Pb-Pb ages of chondrules suggests that the last closure event of the metal and chondrule formation occurred in a common environment (Kleine et al. 2005).

CONCLUSIONS

To explore CB formation conditions, we performed elemental and isotopic measurements of bulk metal phases in two CB_a chondrites, Bencubbin and Gujba, and one CB_b , HaH 237. In addition, we also separated the rim, intermediate, and core fractions of two rounded metal grains from Gujba (CB_a) by sequential digestion and measured the germanium elemental and isotopic compositions of these fractions.

Our petrological observations and in situ elemental analyses suggest that large metal grains formed by the aggregation of smaller grains. In situ analyses of HSEs (Re, W, Os, Ir, Ru, Mo, Pt, Rh) in large metal grains also reveal intra-grain variations that contradict an origin by condensation and diffusive chemical homogenization. We therefore suggest that the HSE compositions of large metal grains result from the aggregation of smaller, prehomogenized grains that formed at various gas pressures and cooling rates in a turbulent impact plume.

The $\delta^{74/70}\text{Ge}$ values observed in the bulk metal of HaH 237 (CB_b) are negative ($\delta^{74/70}\text{Ge} = -0.65 \pm 0.1\%$), whereas those in the bulk metal of CB_a chondrites are positive ($\delta^{74/70}\text{Ge} \approx 1.04 \pm 0.09\%$ for Bencubbin bulk metal). We interpret this difference in bulk metal isotopic compositions in terms of cooling rates during condensation in the impact plume, with HaH 237 experiencing fast cooling rates and nonequilibrium kinetic condensation, and thus acquiring negative $\delta^{74/70}\text{Ge}$ values. In contrast, CB_a metal grains experienced slow cooling rates and near-equilibrium condensation, thus acquiring positive $\delta^{74/70}\text{Ge}$ values. In agreement with previous studies, our data suggest that CB_b metal grains formed under a steep thermal gradient in the external part of the impact plume, whereas CB_a metal grains formed at higher temperatures in the inner part of the plume. Such a heterogeneous plume implies constraints on pressure, and thus on the growth rate of

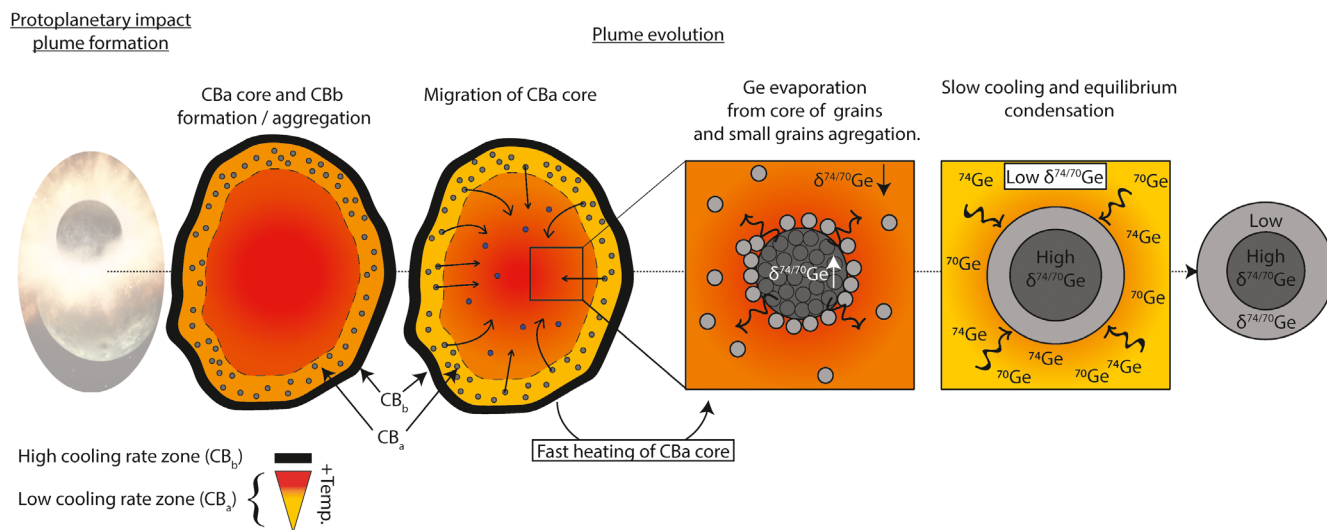


Fig. 9. Sketch figure that sums up CB chondrite formation model from protoplanetary impact and the subsequent plume evolution in function of the cooling rate. Qualitative variations in germanium isotopic composition within the plume and in the final metal grains are highlighted.

metal grains during condensation. We calculated growth rates of 1.40 and 14.08 $\mu\text{m h}^{-1}$ for CB_b and CB_a metal grains, respectively.

We have shown that $\delta^{74/70}\text{Ge}$ values and Ge contents decrease from the core to the rim of Gujba metal grains (CB_a). These zonations cannot result from the diffusion of Ge through metal grains. We propose that these zonations result from near-equilibrium condensation and record plume heterogeneities due to Ge evaporation from metal nuclei. We developed a model in which (1) small metal grains formed under equilibrium; (2) these small grains were then transported to a warmer region of the plume, where they experienced fast partial evaporation of Ge; (3) this kinetic evaporation increased the isotopic compositions of the metallic grains; (4) under high dust pressure and temperatures below those of Fe-Ni condensation, these small grains acted as nuclei for metal condensation and aggregation, thus preventing a total loss of Ge by evaporation; and (5) Ge evaporation from the metal grains enriched the plume in light Ge isotopes, which was recorded by the isotopic compositions of subsequently condensed, more external layers of the metal grains. This model (Fig. 9) explains the lighter Ge isotopic compositions of external layers in metal grains compared to their cores.

Acknowledgments—We thank Damien Cividini for valuable assistance on the NeptunePlus MC-ICP-MS and advice for modifying the germanium chemistry at CRPG-Nancy, and Yoann Greau and Timothy Murphy for their help and advice during analyses at Macquarie University. We are grateful to Joachim Karl for

providing a sample of Hammadah al Hamra 237, and to T. McCoy and J. Hoskin (Department of Mineral Sciences, Smithsonian National Museum of Natural History) for access to their Bencubbin and Gujba samples. Robert Dennen is thanked for his careful correction of the manuscript. We thank Prof. Alex Ruzicka for editorial handling, and Drs. Richard J. Walker and Michael K. Weisberg for their thorough and constructive reviews that helped to improve the manuscript. This is CRPG contribution no. 2769.

Data Availability Statement—The data that support the findings of this study are available in the supplementary material of this article.

Editorial Handling—Prof. Alexander Ruzicka

REFERENCES

- Alard O., Griffin W. L., Lorand J. P., Jackson S. E., and O'Reilly S. Y. 2000. Non-chondritic distribution of the highly siderophile elements in mantle sulphides. *Nature* 407:891–894.
- Anders E. and Grevesse N. 1989. Abundances of the elements: Meteoritic and solar. *Geochimica et Cosmochimica Acta* 53:197–214.
- Bollard J., Connelly J. N., and Bizzarro M. 2015. Pb-Pb dating of individual chondrules from the CB a chondrite Gujba: Assessment of the impact plume formation model. *Meteoritics & Planetary Science* 50:1197–1216.
- Campbell A. J., Humayun M., and Weisberg M. K. 2000. Siderophile-element distributions in zoned metal grains in Hammadah Al Hamra 237. *Meteoritics & Planetary Science* 35:A38.
- Campbell A. J., Humayun M., Meibom A., Krot A. N., and Keil K. 2001. Origin of zoned metal grains in the QUE

- 94411 chondrite. *Geochimica et Cosmochimica Acta* 65:163–180.
- Campbell A. J., Humayun M., and Weisberg M. K. 2002. Siderophile element constraints on the formation of metal in the metal-rich chondrites Bencubbin, Weatherford, and Gujba. *Geochimica et Cosmochimica Acta* 66:647–660.
- Campbell A. J., Zanda B., Perron C., Meibom A., and Petaev M. I. 2005. Origin and thermal history of Fe-Ni metal in primitive chondrites. In *Chondrites and the protoplanetary disk*, edited by Krot A. N., Scott E. R. D., and Reipurth B. San Francisco, California: Astronomical Society of the Pacific. pp. 407–431.
- Campbell D. R. 1975. Isotope effect for self-diffusion in Ge. *Physical Review B* 12:2317–2324.
- Chou C.-L. and Cohen A. J. 1973. Gallium and germanium in the metal and silicates of L- and LL-chondrites. *Geochimica et Cosmochimica Acta* 37:315–327.
- Connelly J. N., Bizzarro M., Krot A. N., Nordlund A., Wielandt D., and Ivanova M. A. 2012. The absolute chronology and thermal processing of solids in the solar protoplanetary disk. *Science* 338:651–655.
- Escoube R., Rouxel O. J., Luais B., Ponzevera E., and Donard O. F. X. 2012. An intercomparison study of the germanium isotope composition of geological reference materials. *Geostandards and Geoanalytical Research* 36:149–159.
- Fedkin A. V., Grossman L., Humayun M., Simon S. B., and Campbell A. J. 2015. Condensates from vapor made by impacts between metal-, silicate-rich bodies: Comparison with metal and chondrules in CB chondrites. *Geochimica et Cosmochimica Acta* 164:236–261.
- Fegley B. and Palme H. 1985. Evidence for oxidizing conditions in the solar nebula from Mo and W depletions in refractory inclusions in carbonaceous chondrites. *Earth and Planetary Science Letters* 72:311–326.
- Florin G., Luais B., Rushmer T., and Alard O. 2020. Influence of redox processes on the germanium isotopic composition of ordinary chondrites. *Geochimica et Cosmochimica Acta* 269:270–291.
- Gilbert S., Danyushevsky L., Robinson P., Wohlgemuth-Ueberwasser C., Pearson N., Savard D., Norman M., and Hanley J. 2013. A comparative study of five reference materials and the Lombard meteorite for the determination of the platinum-group elements and gold by LA-ICP-MS. *Geostandards and Geoanalytical Research* 37:51–64.
- Gilmour J. D., Crowther S. A., Busfield A., Holland G., and Whitby J. A. 2009. An early I-Xe age for CB chondrite chondrule formation, and a re-evaluation of the closure age of Shallowater enstatite. *Meteoritics & Planetary Science* 44:573–579.
- Griffin W. L., Powell W. J., Pearson N. J., and O'Reilly S. Y. 2008. GLITTER: Data reduction software for laser ablation ICP-MS. In *Laser ablation-ICP-MS in the earth sciences*, edited by Sylvester P. Mineralogical Association of Canada, Short Course Series 40, Quebec, Canada: Mineralogical Association of Canada, 204–207.
- Grossman J. N. and Zipfel J. 2001. The Meteoritical Bulletin, No. 85. *Meteoritics & Planetary Science* 36:A293–A322.
- Grossman J., Rubin A., and Macpherson G. 1988. ALH 85085: A unique volatile-poor carbonaceous chondrite with possible implications for nebular fractionation processes. *Earth and Planetary Science Letters* 91:33–54.
- Ivanova M. A., Kononkova N. N., Krot A. N., Greenwood R. C., Franchi I. A., Verchovsky A. B., Trieloff M., Korochantseva E. V., and Brandstätter F. 2008. The Isheyevo meteorite: Mineralogy, petrology, bulk chemistry, oxygen, nitrogen, carbon isotopic compositions, and ^{40}Ar - ^{39}Ar ages. *Meteoritics & Planetary Science* 43:915–940.
- Kallemeyn G. W., Boynton W. V., Willis J., and Wasson J. T. 1978. Formation of the Bencubbin polymict meteoritic breccia. *Geochimica et Cosmochimica Acta* 42:507–515.
- Kallemeyn G. W., Rubin A. E., and Wasson J. T. 2001. Compositional studies of Bencubbin dark silicate host and an OC clast: Relationships to other meteorites and implications for their origin (abstract #2070). 32nd Lunar and Planetary Science Conference. CD-ROM.
- Kleine T., Mezger K., Palme H., Scherer E., and Münker C. 2005. Early core formation in asteroids and late accretion of chondrite parent bodies: Evidence from 182Hf-182W in CAIs, metal-rich chondrites, and iron meteorites. *Geochimica et Cosmochimica Acta* 69:5805–5818.
- Krot A. N., Meibom A., Petaev M. I., Keil K., Zolensky M. E., Saito A., Mukai M., and Ohsumi K. 2000a. Ferrous silicate spherules with euhedral iron-nickel metal grains from CH carbonaceous chondrites: Evidence for supercooling and condensation under oxidizing conditions. *Meteoritics & Planetary Science* 35:1249–1258.
- Krot A. N., Meibom A., and Keil K. 2000b. Volatile-poor chondrules in CH carbonaceous chondrites: Formation at high ambient nebular temperature (abstract #1481). 31st Lunar and Planetary Science Conference. CD-ROM.
- Krot A. N., Meibom A., Weisberg M. K., and Keil K. 2002. The CR chondrite clan: Implications for early solar system processes. *Meteoritics & Planetary Science* 37:1451–1490.
- Krot A. N., Amelin Y., Cassen P., and Meibom A. 2005. Young chondrules in CB chondrites from a giant impact in the early solar system. *Nature* 436:989–992.
- Lodders K. 2003. Solar system abundances and condensation temperatures of the elements. *The Astrophysical Journal* 591:1220–1247.
- Lodders K., Palme H., and Gail H. 2009. Abundances of the elements in the solar system. In *Solar system*, edited by Trümperp J. E. New York: Springer-Verlag. pp. 560–630.
- Luais B. 2007. Isotopic fractionation of germanium in iron meteorites: Significance for nebular condensation, core formation and impact processes. *Earth and Planetary Science Letters* 262:21–36.
- Luais B. 2012. Germanium chemistry and MC-ICPMS isotopic measurements of Fe-Ni, Zn alloys and silicate matrices: Insights into deep Earth processes. *Chemical Geology* 334:295–311.
- Luais B., Gondoin T., De Gournay T., and Cividini D. 2017. Origin of pallasites from chemical and isotopic composition of siderophile and volatile element. Goldschmidt2017 Abstract, Paris.
- Meibom A., Petaev M. I., Krot A. N., Wood J. A., and Keil K. 1999. Primitive FeNi metal grains in CH carbonaceous chondrites formed by condensation from a gas of solar composition. *Journal of Geophysical Research: Planets* 104:22,053–22,059.
- Meibom A., Desch S. J., Krot A. N., Cuzzi J. N., Petaev M. I., Wilson L., and Keil K. 2000. Large-scale thermal events in the solar nebula: Evidence from Fe, Ni metal grains in primitive meteorites. *Science* 288:839–841.

- Meibom A., Richter K., Chabot N., Dehn G., Antignano A., McCoy T. J., Krot A. N., Zolensky M. E., Petaev M. I., and Keil K. 2005. Shock melts in QUE 94411, Hammadah al Hamra 237, and Bencubbin: Remains of the missing matrix? *Meteoritics & Planetary Science* 40:1377–1391.
- Mullane E., Alard O., Gounelle M., and Russell S. S. 2004. Laser ablation ICP-MS study of IIIAB irons and pallasites: Constraints on the behaviour of highly siderophile elements during and after planetesimal core formation. *Chemical Geology* 208:5–28.
- Newsom H. E. and Drake M. J. 1979. The origin of metal clasts in the Bencubbin meteoritic breccia. *Geochimica et Cosmochimica Acta* 43:689–707.
- Okabayashi S., Yokoyama T., Nakanishi N., and Iwamori H. 2019. Fractionation of highly siderophile elements in metal grains from unequilibrated ordinary chondrites: Implications for the origin of chondritic metals. *Geochimica et Cosmochimica Acta* 244:197–215.
- Petaev M. I., Meibom A., Krot A. N., Wood J. A., and Keil K. 2001. The condensation origin of zoned metal grains in Queen Alexandra Range 94411: Implications for the formation of the Bencubbin-like chondrites. *Meteoritics & Planetary Science* 36:93–106.
- Pravdivtseva O., Meshik A., Hohenberg C. M., Krot A. N., and Amelin Y. 2014. I-Xe age of a non-porphyritic magnesian chondrule from the Hammadah al Hamra 237 CB carbonaceous chondrite: Validation of absolute I-Xe ages (abstract #2456). 45th Lunar and Planetary Science Conference. CD-ROM.
- Richter F. M. 2004. Timescales determining the degree of kinetic isotope fractionation by evaporation and condensation. *Geochimica et Cosmochimica Acta* 68:4971–4992.
- Richter F. M., Dauphas N., and Teng F.-Z. 2009. Non-traditional fractionation of non-traditional isotopes: Evaporation, chemical diffusion and Soret diffusion. *Chemical Geology* 258:92–103.
- Richter F. M., Huss G. R., and Mendybaev R. A. 2014. Iron and nickel isotopic fractionation across metal grains from three CBb (abstract #1346). 45th Lunar and Planetary Science Conference. CD-ROM.
- Richter K., Campbell A. J., and Humayun M. 2005. Diffusion of trace elements in FeNi metal: Application to zoned metal grains in chondrites. *Geochimica et Cosmochimica Acta* 69:3145–3158.
- Rouxel O. J. and Luais B. 2017. Germanium isotope geochemistry. *Reviews in Mineralogy and Geochemistry* 82:601–656.
- Rubin A. E., Kallemeyn G. W., Wasson J. T., Clayton R. N., Mayeda T. K., Grady M., Verchovsky A. B., Eugster O., and Lorenzetti S. 2003. Formation of metal and silicate globules in Gujba: A new Bencubbin-like meteorite fall. *Geochimica et Cosmochimica Acta* 67:3283–3298.
- Schaudy R., Wasson J. T., and Buchwald V. F. 1972. The chemical classification of iron meteorites: VI. A reinvestigation of iron with Ge concentration lower than 1 ppm. *Icarus* 17:174–192.
- Scott E. R. D. and Wasson J. T. 1976. Chemical classification of iron meteorites: VIII. Groups IC, IIE, IIIF and 97 other irons. *Geochimica et Cosmochimica Acta* 40:103–115.
- Sears D. W. 1978. Condensation and the composition of iron meteorites. *Earth and Planetary Science Letters* 41:128–138.
- Vogel G., Hettich G., and Mehrer H. 1983. Self-diffusion in intrinsic germanium and effects of doping on self-diffusion in germanium. *Journal of Physics C: Solid State Physics* 16:6197–6204.
- Wai C. M. and Wasson J. T. 1979. Nebular condensation of Ga, Ge and Sb and the chemical classification of iron meteorites. *Nature* 282:790.
- Walker R. J., McDonough W. F., Honesto J., Chabot N. L., McCoy T. J., Ash R. D., and Bellucci J. J. 2008. Modeling fractional crystallization of group IVB iron meteorites. *Geochimica et Cosmochimica Acta* 72:2198–2216.
- Walter M. J., Newsom H. E., Ertel W., and Holzheid A. 2000. Siderophile elements in the Earth and Moon: Metal/silicate partitioning and implications for core formation. In *Origin of the Earth and Moon*, edited by Canup R. M. and Richter K. Tucson, Arizona: The University of Arizona Press. pp. 265–289.
- Wasson J. T. 1969. The chemical classification of iron meteorites: III. Hexahedrites and other irons with germanium concentrations between 80 and 200 ppm. *Geochimica et Cosmochimica Acta* 33:859–876.
- Wasson J. T. 1974. *Meteorites: Classification and properties*. Berlin: Springer-Verlag. 318 p.
- Wasson J. T. and Schaudy R. 1971. The chemical classification of iron meteorites: V groups IIIC and IIID and other irons with germanium concentrations between 1 and 25 ppm. *Icarus* 14:59–70.
- Weisberg M. K. and Kimura M. 2010. Petrology and Raman spectroscopy of high pressure phases in the Gujba CB chondrite and the shock history of the CB parent body. *Meteoritics & Planetary Science* 45:873–884.
- Weisberg M. K., Prinz M., and Nehru C. E. 1990. The Bencubbin chondrite breccia and its relationship to CR chondrites and the ALH 85085 chondrite. *Meteoritics* 25:269–279.
- Weisberg M. K., Prinz M., Clayton R. N., Mayeda T. K., Grady M. M., and Pillinger C. T. 1995. The CR chondrite clan. *Antarctic Meteorite Research* 8:11.
- Weisberg M. K., Prinz M., Clayton R. N., Mayeda T. K., Sugiura N., Zashu S., and Ebihara M. 1999. QUE 94411 and the origin of Bencubbinites (abstract #1416). 30th Lunar and Planetary Science Conference. CD-ROM.
- Weisberg M. K., Prinz M., Clayton R. N., Mayeda T. K., Sugiura N., Zashu S., and Ebihara M. 2001. A new metal-rich chondrite grouplet. *Meteoritics & Planetary Science* 36:401–418.
- Weyrauch M., Zipfel J., and Weyer S. 2019. Origin of metal from CB chondrites in an impact plume—A combined study of Fe and Ni isotope composition and trace element abundances. *Geochimica et Cosmochimica Acta* 246:123–137.
- Wohlgenuth-Ueberwasser C. C., Ballhaus C., Berndt J., Stotter née Paliulionyte V., and Meisel T. 2007. Synthesis of PGE sulfide standards for laser ablation inductively coupled plasma mass spectrometry (LA-ICP-MS). *Contributions to Mineralogy and Petrology* 154:607–617.
- Wood B. J., Smythe D. J., and Harrison T. 2019. The condensation temperatures of the elements: A reappraisal. *American Mineralogist* 104:844–856.
- Yamashita K., Maruyama S., Yamakawa A., and Nakamura E. 2010. ^{53}Mn – ^{53}Cr chronometry of CB chondrite: Evidence for uniform distribution of ^{53}Mn in the early solar system. *The Astrophysical Journal* 723:20–24.
- Yasui C., Kobayashi N., Tokunaga A. T., and Saito M. 2014. Rapid evolution of the innermost dust disk of

protoplanetary disks surrounding intermediate-mass stars. *Monthly Notices of the Royal Astronomical Society* 442:2543–2559.

Zhang J., Williams D. B., and Goldstein J. I. 1993. The microstructure and formation of duplex and black plesite in iron meteorites. *Geochimica et Cosmochimica Acta* 57:3725–3735.

Zhu K., Liu J., Moynier F., Qin L., Alexander C. M. O'D., and He Y. 2019. Chromium isotopic evidence for an early

formation of chondrules from the Ornans CO chondrite. *The Astrophysical Journal* 873:82.

Zipfel J. and Weyer S. 2007. In situ analyses of Fe isotopes in zoned metal grains of Hammadah Al Hamra 237 (abstract #1927). 38th Lunar and Planetary Science Conference. CD-ROM.

Zipfel J., Wlotzka F., and Spettel B. 1998. Bulk chemistry and mineralogy of a new “unique” metal-rich chondritic breccia, Hammadah Al Hamra 237. 29th Lunar and Planetary Science Conference. CD-ROM.

SUPPORTING INFORMATION

Additional supporting information may be found in the online version of this article.

Fig. S1. Comparison of Ir, Os, and Au concentrations obtained for all LA-ICP-MS spots of metal of Bencubinite samples, using PGE-A and FeS1 standards. The black line is the x=y line.

Fig. S2. Cross sections of moderately volatile element contents in a metal grain from Gujba, normalized to CI chondrite (left) and Ni content (right).

Fig. S3. $\delta^{72/70}\text{Ge}$ vs $\delta^{74/70}\text{Ge}$ diagram for the analyzed CB samples. All data plot on the mass-dependent fractionation line, demonstrating the accuracy of our measurements. Diamonds represent sequentially digested Gujba metal fractions (R, rim; I, intermediate; C, core) and circles are the Bencubbin and HaH 237 bulk metal compositions.

Fig. S4. AG 50W-X8 elution curves for ~35 μg of Ge of Magura iron meteorite solution as a function of

the volume of 0.5 M HNO_3 eluted from the column. The first 2.5 ml corresponds to sample loading and the dead volume of the resin. Only germanium is eluted at this molarity. Note that a very small amount of Zn, corresponding to less than 0.01%, of the total amount loaded, and insignificant amount of Ga are eluted at around 6 and 10 mL eluant volume.

Table S1. Comparison between LA-ICP-MS measurements from this study and Walker et al. (2008), Gilbert et al. (2013) values for NIST1158, PGE-A synthetic standard as well as Filomena and Hoba iron meteorites. Errors associated to each value are given as 1SD.

Table S2. Error in percent and detection limits in ppm for LA-ICP-MS measurements, calculated as the mean background multiplied by 3 times the standard deviation.

Table S3. Elemental composition in ppm (except Ni in %) of metal grains in Gujba, Bencubbin (Ben) and HaH 237 (HaH). Elements are classified in function of their volatilities. B.L.: below detection limit.